N73-17504
NASA CR-2203

CASE FILE COPY

SHORT AND LONG PERIOD ATMOSPHERIC VARIATIONS BETWEEN 25 AND 200 KM

by C. G. Justus and Arthur Woodrum

Prepared by
SCHOOL OF AEROSPACE ENGINEERING
GEORGIA INSTITUTE OF TECHNOLOGY
Atlanta, Ga. 30332
for George C. Marshall Space Flight Center

1. REPORT NO. NASA CR-2203	2. GOVERNMENT ACCESSION NO.	3. RECIPIENT'S CATALOG NO.
4. TITLE AND SUBTITLE SHORT AND LONG PERIOD ATMOSPHERIC VARIATIONS BETWEEN 25 and 200 KM		5. REPORT DATE February 1973
		6. PERFORMING ORGANIZATION CODE M112
7. AUTHOR(S) C. G. Justus and Arthur Woodrum		8. PERFORMING ORGANIZATION REPORT # E-16-612
9. PERFORMING ORGANIZATION NAME AND ADDRESS School of Aerospace Engineering Georgia Institute of Technology Atlanta, Georgia 30332		10. WORK UNIT NO.
		11. CONTRACT OR GRANT NO. NAS8-26658
		13. TYPE OF REPORT & PERIOD COVERED
12. SPONSORING AGENCY NAME AND ADDRESS National Aeronautics and Space Administration Washington, D. C. 20546		CONTRACTOR REPORT
		14. SPONSORING AGENCY CODE

15. SUPPLEMENTARY NOTES
Prepared under the technical monitorship of Mr. Robert E. Smith, Aerospace Environment Division, Aero-Astrodynamics Laboratory, NASA-Marshall Space Flight Center.

16. ABSTRACT

This report extends and revises the first project report NASA-CR-2062 on this contract. Previously collected data on atmospheric pressure, density, temperature and winds between 25 and 200 km from sources including Meteorological Rocket Network data, ROBIN falling sphere data, grenade release and pitot tube data, meteor winds, chemical release winds, satellite data, and others were analyzed by a daily difference method and results on the distribution statistics, magnitude, and spatial structure of gravity wave and planetary wave atmospheric variations are presented. Time structure of the gravity wave variations were determined by the analysis of residuals from harmonic analysis of time series data. Planetary wave contributions in the 25-85 km range were discovered and found to have significant height and latitudinal variation. Long period planetary waves, and seasonal variations were also computed by harmonic analysis. Revised height variations of the gravity wave contributions in the 25 to 85 km height range were computed. It was determined that, on the average, gravity wave energy deposition or reflection occurs at all altitudes except the 55 to 75 km region of the mesosphere. An engineering method and design values for gravity wave magnitudes and wave lengths are given to be used for such tasks as evaluating the effects on the dynamical heating, stability and control of spacecraft such as the Space Shuttle vehicle in launch or re-entry trajectories.

17. KEY WORDS Density, Wind Variations 25-200 km	18. DISTRIBUTION STATEMENT

19. SECURITY CLASSIF. (of this report) Uncl	20. SECURITY CLASSIF. (of this page) Uncl	21. NO. OF PAGES 86	22. PRICE $3.00

TABLE OF CONTENTS

ACKNOWLEDGMENTS

1. INTRODUCTION

The variations of the upper atmosphere are due to a wide variety of sources and cover a broad range of frequencies and size scales. The shortest period, smallest scale variations are due to turbulence. Certain variations of only slightly longer period and larger scale are thought to be due to the action of gravity waves. For a review of the evidence for gravity waves and the possible mechanisms for generation and dissipation of gravity waves see the previous report by Justus and Woodrum[1]. There has been no unambiguous resolution of gravity waves in the upper atmosphere (i.e. simultaneous observation of amplitudes, phases, and frequency sufficient to verify propagation according to the theoretical dispersion equation). However, there is strong circumstantial evidence for their occurrence and the short period (i.e. < 24 hr) irregular variations discussed in this report may be assumed to result from gravity waves.

Atmospheric tides cause variations with periods of 24 hours and harmonics (e.g. 12 and 8 hours). The strongest tidal influence comes from solar heating, but lunar tides also exist similar to those produced in the ocean. For a review of theory and observations of atmospheric tides see the book by Lindzen and Chapman[2].

Longer period phenomena are the result of synoptic variations and planetary scale waves. Although planetary waves have been resolved up to about 30 km[3], their propagation to higher altitudes has been somewhat uncertain prior to this report. Still longer period phenomena are the seasonal, semi-annual, annual, and quasi-biennial oscillations.

This report is a continuation and revision of results reported earlier[1]. Two analysis techniques are used to study gravity wave, planetary wave, and long period variations. The first method, known as the daily difference technique was developed[4,5] for application to upper atmosphere data where specific removal of long period and tidal variations would be difficult because of lack of data. This approach allows for the estimation of magnitudes, probability distributions, and vertical structure functions of the irregular variations of less than one pay period. It also can be used to determine the magnitude of the variations due to planetary waves of periods up to a few days. The second data analysis technique is harmonic analysis of time series data. This approach can be used, when sufficient data exists, to estimate tides, and long period variations such as annual and quasi-biennial oscillations.

The purpose of this report is two fold: first to present the results of an investigation of the effects of gravity waves, tides, and planetary waves in producing upper atmospheric variations, and second to summarize the results in such a fashion that they can be used in engineering design problems, in particular the effects of the atmospheric variations on the stability, control, and dynamic heating of the space shuttle vehicle.

2. DATA ANALYSIS AND INTERPRETATION

Structure Functions. An alternate form of the correlation function known as the structure function was first used extensively by Russian meteorologists in the analysis of turbulence. The structure function of a statistically stationary time varying process f(t) is given by

$$D(\tau) = \langle [f(t + \tau) - f(t)]^2 \rangle \qquad (1)$$

where the structure function D depends only on the time displacement τ because of the statistical stationarity. The angle brackets in (1) denote averaging.

Structure function analysis can be applied to wave phenomena also. Consider the process f(t) to be a wave of frequency ω and amplitude A, i.e. f(t) = A sin ($\omega t + \alpha$), where α is a phase angle. If the averaging process is taken to be integration over any whole number of periods, where the period T = $2\pi/\omega$, then the mean square value of f(t) is $\langle f^2 \rangle = A^2/2$. It is also easy to determine that the structure function in this case is given by $D(\tau) = A^2 (1 - \cos \omega\tau)$. Thus the structure function of a single component wave field has the properties of being proportional to τ^2 for very small time displacement τ since the leading term in $1 - \cos \omega\tau$ is $\omega^2\tau^2/2$, and being periodic with the same frequency ω as the wave. Notice that the first maximum in $D(\tau)$ would occur at $\tau = \pi/\omega = T/2$, so the first maximum occurs at the half period value. The value of the maximum is $2A^2$.

The structure function analysis of waves can easily be extended to a set of waves which are part of a harmonic series. Consider f(t) to be periodic with period T and to be made up of N different waves each wave n having a fre-

quency $\omega_n = 2n\pi/T$, i.e.

$$f(t) = \Sigma A_n \sin (\omega_n t + \alpha_n) \tag{2}$$

where the summation is from n = 1 to n = N. Using the same type of averaging by integrating as on the single wave, one can determine that the mean square value of f is given by

$$\langle f^2 \rangle = \Sigma A_n^2/2 \tag{3}$$

and that the structure function is given by

$$D(\tau) = \Sigma A_n^2 (1 - \cos \omega_n \tau) \tag{4}$$

Thus again the behavior at small time displacement is proportional to τ^2, since the leading term in (4) is $\Sigma A_n^2 \omega_n^2 \tau^2/2$. The structure function in this case is again periodic with period T and has components with amplitudes related to the square of the amplitudes of the corresponding frequencies in the process f(t).

If the process f(t) is made up of sufficient components that it must be considered as having a continuous spectrum of amplitudes $A(\omega)$ (as is the case with turbulence and may also be the case when gravity wave modes have significant nonlinear modal interaction) then f(t) can be represented by

$$f(t) = \int_{-\infty}^{\infty} A(\omega) e^{i\omega t} d\omega \tag{5}$$

(For a more rigorous discussion of spectral representation see Lumley and Panofsky[6] and Lin[7]. The mean square value of f(t) is given by

4

$$\langle f^2 \rangle = 2 \int_{-\infty}^{\infty} \phi(\omega) \, d\omega \tag{6}$$

where $\phi(\omega)$ is the spectral density of the mean square variations of $f(t)$. The structure function is given by

$$D(\tau) = 2 \int_{0}^{\infty} \phi(\omega) \, (1 - \cos \omega\tau) \, d\omega \tag{7}$$

Again the initial variation of $D(\tau)$ for small time displacements is proportional to τ^2 since

$$D(\tau) = [\int_{0}^{\infty} \omega^2 \phi(\omega) \, d\omega] \, \tau^2 \qquad \tau \to 0 \tag{8}$$

However, at large time displacements $D(\tau)$ is not periodic but approaches a constant value of $2\langle f^2 \rangle$. This is seen readily from the fact that $D(\tau)$ is related to the correlation function $\rho(\tau)$ by

$$D(\tau) = 2\langle f^2 \rangle \, [1 - \rho(\tau)] \tag{9}$$

for all stationary processes $f(t)$. Hence, because $\rho(\tau)$ approaches 0 for large τ, then

$$D(\tau) = 2 \langle f^2 \rangle \qquad \tau \to \infty \tag{10}$$

In addition, if there is an appreciable range of frequencies over which $\phi(\omega)$ varies as a power law

$$\phi(\omega) = C \, \omega^{-a} \tag{11}$$

then there is a range of time displacements over which

$$D(\tau) \simeq C[\int_o^\infty x^{-a} (1 \cos x) dx] \tau^{a-1} \tag{12}$$

where $x = \omega\tau$ and the integral in brackets is some definite constant value. Thus observed power law behavior of the structure function (i.e. $a - 1$) can be related to the power law of the spectral density (i.e. $-a$).

As an example of how the integral time scale $T = \int_o^\infty \rho(\tau) d\tau$ can be obtained from the time structure function, consider the case in which the correlation $\rho(\tau)$ of the process $f(t)$ is given by $\exp(-\tau/T)$. For this particular case the small time behavior of the structure function is $D(\tau) \simeq 2<f^2> \tau/T$. If this early time period slope is extrapolated to intersect with a similar extrapolation of the long time variation, $D(\tau) \simeq 2<f^2>$, the graphical intersection point occurs at a value $\tau = T$. Similar graphical techniques can be devised to determine integral scales if different correlation functions, with different early time behavior, apply. Also similar techniques can be used with spatial structure functions to estimate size scales (see section 8).

Daily Difference Analysis. The daily difference analysis technique was developed[4,5] for applications where limited data did not allow explicit separation of the tidal components in order to determine the small scale irregular variations. As an example of the application of this technique consider a vertical profile of a parameter $F(z, t)$ over height z at time t where F may be a wind component, pressure, density, or temperature. We consider that F is made up of a prevailing value $F_o(z)$ which is time invariant, plus a long period (e.g. seasonal, annual, or quasi-biennial oscillation) component $S(z, t)$, a planetary scale or synoptically varying component $P(z, t)$, a tidal component $T(z, t)$, a gravity wave or short period irregular

6

component G(z, t), and a still smaller scale component made up of measurement error and turbulence E(z, t). Thus

$$F(z, t) = F_o(z) + S(z, t) + P(z, t) + T(z, t)$$
$$+ G(z, t) + E(z, t) \qquad (13)$$

The component P(z, t) would be composed of traveling waves only, all truly standing waves would be included in the component $F_o(z)$ or seasonally fluctuating standing waves would be included in S(z, t). We now choose two profiles of F at times t_1 and t_2 such that $t_2 - t_1 = \Delta t = 24n$ hours where n is an integer. If, at any selected altitude z, we difference the corresponding value of F then

$$\Delta F_n(z) = F(z, t_2) - F(z, t_1) = [S(z, t_2) - S(z, t_1)]$$
$$+ [P(z, t_2) - P(z, t_1)] + [T(z, t_2) - T(z, t_1)]$$
$$+ [G(z, t_2) - G(z, t_1)] + [E(z, t_2) - E(z, t_1)] \qquad (14)$$

We now make the following assumptions: (1) Assume that n is sufficiently small that $S(z, t_2) \simeq S(z, t_1)$ (i.e. n is a small number of days compared to times over which appreciable seasonal variation would occur). In the analysis we restricted n to 15 or less days. (2) Assume that because the tidal component is diurnally repeating and Δt is a multiple of 24 hours that $T(z, t_2) = T(z, t_1)$. (Any systemmatic or synoptic variation in the tidal parameters would be included in the component P and the seasonal variation of the tides would be included in the component S). (3) The planetary scale, gravity wave and error components are uncorrelated with each other and are corre-

7

lated only with themselves (autocorrelation). Equation (13) can now be squared and averaged over an ensemble of different profile pairs all having the same time separation Δt. The result is

$$
\begin{aligned}
<[\Delta F_n(z)]^2> &= <[P(z, t_2) - P(z, t_1)]^2> \\
&+ <[G(z, t_2) - G(z, t_1)]^2> + <[E(z, t_2) - E(z, t_1)]^2>
\end{aligned} \tag{15}
$$

The cross product terms in (15) have dropped out because of assumption 3 above. If equation (15) is now expanded and the mean square values of P, G, and E are assumed to be independent of time (i.e. statistically stationary) then the mean square data differences become

$$
\begin{aligned}
<[\Delta F_n(z)]^2> &= 2<P^2(z)> [1 - \rho_P(\Delta t)] \\
&+ 2<G^2(z)> [1 - \rho_G(\Delta t)] + 2<E^2(z)> [1 - \rho_E(\Delta t)]
\end{aligned} \tag{16}
$$

where ρ_P, ρ_G, and ρ_E are the time autocorrelation functions of P, G, and E respectively. The following assumptions are now made about the periods of the various remaining components: (1) the gravity wave, error and turbulence components are uncorrelated for all time differences of 1 day or more (i.e. $n \geq 1$), (2) the planetary wave component is of such a long period that $\rho_P(\Delta t) \simeq 1$ for $\Delta t = 1$ day, but for large n the planetary wave component also becomes uncorrelated. Thus for single day differences, equation (16) becomes

$$
<[\Delta F_1(z)]^2> = 2[<G^2(z)> + <E^2(z)>] \tag{17}
$$

that is, the mean square differences in the observed data are equal to twice the mean square magnitude of the gravity wave component (plus any contribution from measurement errors or small scale turbulence). For time separations of many days (n large, say approaching 15) and under the above assumptions equation (16) becomes

$$<[\Delta F_n(z)]^2> = 2[<P^2(z)> + <G^2(z)> + <E^2(z)>] \qquad (18)$$

thus, at longer time separations the magnitude of the planetary wave contributions becomes added. At intermediate time separations progressively larger portions of the planetary wave contribution (through the factor $1 - \rho_P(\Delta t)$) become added. Equations (17) and (18) can be subtracted, which yields

$$<[\Delta F_n(z)]^2> - <[\Delta F_1(z)]^2> = 2<P^2(z)> \qquad (19)$$

This allows an estimate of the contribution of planetary waves directly from the observed daily differences of measured data and the estimate is unbiased with respect to the error component $<E^2>$ since that component cancels in the subtraction process. Note, however, that this method, like any single site method, does not resolve the standing planetary wave components, only the traveling components.

The assumptions outlined above regarding relative periods of the gravity wave and planetary wave components (and the implicit assumption that the errors are sufficiently small that meaningful results can be obtained from the analysis) are subject to verification. The results presented later in

9

this report do, indeed, confirm these assumptions.

The vertical structure function of the daily differences can also be related to the vertical structure function of the gravity wave component. The vertical structure function of the 1 day differences in the data values is given by

$$D_{\Delta F_1}(\zeta) = <[\Delta F_1(z + \zeta) - \Delta F_1(z)]^2>$$ (20)

Subtraction of the expression

$$\Delta F_1(z) = [G(z, t_2) - G(z, t_1)] + [E(z, t_2) - E(z, t_1)]$$ (21)

and the comparable expression for $\Delta F_1(z + \zeta)$ yields, after some rearrangement

$$D_{\Delta F_1}(\zeta) = <[G(z + \zeta, t_2) - G(z, t_2)]^2>$$

$$+ <[G(z + \zeta, t_1) - G(z, t_1)]^2> + <[E(z + \zeta, t_2) - E(z, t_2)]^2>$$

$$+ <[E(z + \zeta, t_1) - E(z, t_1)]^2>$$ (22)

Several cross product terms in (22) have dropped out because of the lack of correlation between G and E and the lack of time autocorrelation of G and E over periods of 1 day. If the G and E fields are vertically homogeneous, then (22) will depend on ζ only, otherwise it will depend separately on z and ζ. Under the previously employed assumption of statistical stationarity,

10

and under the assumption that the E values are uncorrelated over the height separation ζ, (22) becomes

$$D_{\Delta F_1}(\zeta) = 2<[G(z + \zeta) - G(z)]^2> + 4<E^2>$$

$$= 2 D_G(\zeta) + 4<E^2> \tag{23}$$

Thus the vertical structure function of the single day differences in the data profiles is twice the vertical structure function of the gravity wave component (plus a contribution from error and small scale turbulence).

A similar analysis for vertical structure functions of daily differences of data profiles for Δt a large number of days, (but small compared to the periods in the component S) shows that

$$D_{\Delta F_n}(\zeta) = 2D_P(\zeta) + 2D_G(\zeta) + 4<E^2> \tag{24}$$

The structure function of the planetary wave component can be obtained by differencing (24) and (23).

$$D_{\Delta F_n}(\zeta) - D_{\Delta F_1}(\zeta) = 2D_P(\zeta) \tag{25}$$

In addition to vertical structure functions, horizontal structure functions of the gravity wave components can also be calculated by differencing data from the up and down trail trajectories of rockets or from closely spaced simultaneous observations. It should be noted that the assumption of independence of the gravity wave component profiles G would not be valid in this case, and this type of difference yields a structure function which has significant var-

11

iation with the distance between the places of evaluation of the two profiles. However, since the effects of tides and other phenomena are not removed, the horizontal structure functions yield valid results of truly irregular variations only if the distance between profiles is kept small compared to the horizontal wave lengths of these tides and other phenomena. It should also be noted that the horizontal structure function used for velocity is actually the structure function of the horizontal velocity magnitude

$$D(r) = \left\{ <[u(\underset{\sim}{x} + \underset{\sim}{r}) - u(\underset{\sim}{x})]^2> + <[v(\underset{\sim}{x} + \underset{\sim}{r}) - v(\underset{\sim}{x})]^2> \right\}/2 \qquad (26)$$

where u is the eastward velocity component, v is the northward component, $\underset{\sim}{x}$ is the horizontal vector location of one velocity evaluation, $\underset{\sim}{r}$ is the vector displacement between the locations of velocity evaluation, and r is the magnitude of the vector $\underset{\sim}{r}$. The definition (26) is dependent on the magnitude r and not the direction of the displacement and no separate consideration of longitudinal and transverse structure functions are required. (A longitudinal structure function would be of the form $<[u(x + \Delta x) - u(x)]^2>$ and a transverse structure function would be of the form $<[u(y + \Delta y) - u(y)]^2>$).

Harmonic Analysis. Data from three sites of Meteorological Rocket Network (MRN) data were collected and a harmonic analysis was performed on the data for periods of 5 days to 1000 days. For a particular site, only data obtained at the same time of day were accepted in order that the solar radiation error would be minimized. A function of the following form was fitted to the data by a least squares process:

$$F(t) = A_o + A_1 \sin (2\pi t/P + \phi) \qquad (27)$$

where t is the time, A_o is the mean value of the parameter, A_1 is the amplitude for the oscillation of period P, and ϕ is the phase angle. As the period P was varied from 5 days to 1000 days, a periodicity spectrum was calculated.

Harmonic analysis was performed also on five sets of MRN data for tidal components. In the past, tidal analysis has been performed usually on data obtained from a high density of rocket launches over a basic period of about 48 hours. However, there are frequenctly data from single rocket launches over a period of 5 to 10 days before or after the basic 48 hours. A preliminary error analysis indicates that the error in the harmonic analysis of the tidal components can be reduced significantly if input data includes these scattered data in addition to the data of the basic 48 hours. Solar radiation corrections were applied also to each data set. Then each data set was smoothed by the use of a polynomial smoothing function over five kilometer height intervals. Then, a function of the following form was fitted to the smoothed data by a least squares process:

$$F(t) = A_o + A_{12} \sin (2\pi t/12 + \phi_{12}) + A_{24} \sin (2\pi t/24 + \phi_{24}) \qquad (28)$$

where time t is measured in hours, A_o is the mean value of the parameter, A_{12} and A_{24} are the amplitudes of the 12 hour and 24 hour period tides, ϕ_{12} and ϕ_{24} are phase angles for those tidal components. (The actual least squares fit was done in terms of sine and cosine terms equivalent to (28).) The results of the harmonic analysis were subtracted from the solar radiation corrected data to find residual values. These residual values were evaluated at altitudes of one kilometer increments from a height of 45 km to 60 km. Thus, profiles of irregular variations, or gravity waves, were obtained. These gravity wave profiles were used to compute time structure functions.

3. MAGNITUDES OF GRAVITY WAVE AND PLANETARY WAVE VARIATION

Resolution of the planetary wave component. Characteristics of the magnitude, probability distribution and structure of irregular winds at chemical release altitudes ($\simeq$ 90 - 130 km) were first studied by Woodrum and Justus[4,5]. In this earlier analysis significant variations with height of the rms daily difference winds were observed. However, no variation with number of days separation between profile pairs was observed, and so, according to the concepts discussed in the previous section, it was considered that planetary waves do not propagate to the 90 - 130 km level with sufficient amplitude to be detectable.

In the first part of this study[1] a large number of data in the 25 - 200 km height range from various sources were collected for analysis by the daily difference method. These data included Meteorological Rocket Network, grenade, pitot tube, falling sphere, meteor winds, and satellite measurements as well as chemical release data. (For a complete list of data sources and references see the earlier report[1].) For the first phase of this study the daily difference analysis was performed by computing mean square daily differences and averaging over all days of separation between 1 and 15.

For the present phase of the study daily differences were computed separately for each day of separation in order to determine if planetary wave contributions could be detected. The results are shown in Figure 1. This figure shows the mean square daily differences in the 45 - 65 km region, plotted versus number of days separation from 1 to 15, as a time structure function, i.e. $2\sigma^2$ values versus time.
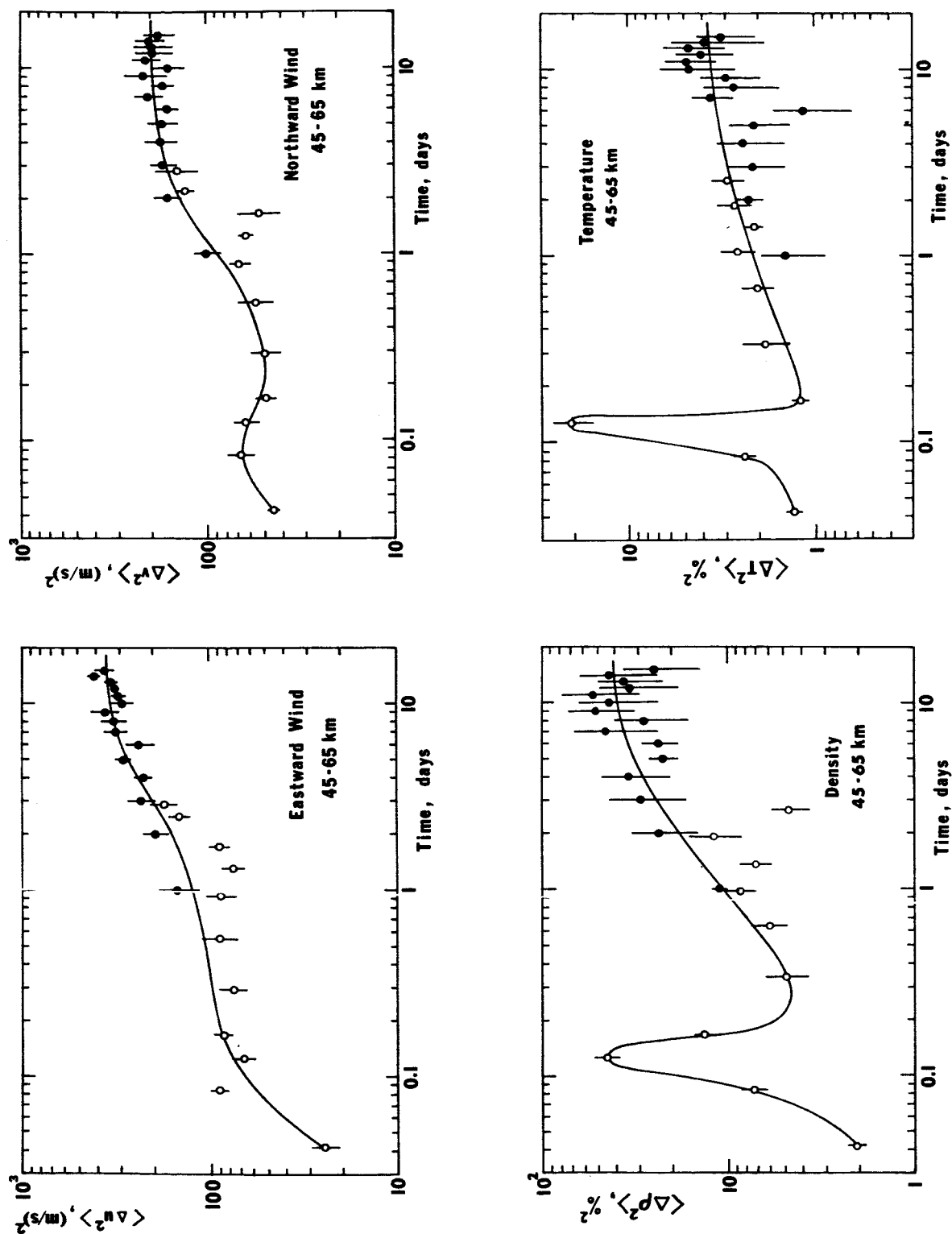
Figure 1. Time structure functions over the range one to 15 days. Solid dots are from daily difference analysis and open circles from residuals after least squares tidal fit to time series data.

15

At the earlier times (1 to 72 hours) in Figure 1 actual time structure functions of the residual winds and thermodynamic variables from the tidal analysis are plotted. The tidal analysis is discussed more fully in Section 5. The time structure data from the residual winds of the tidal analysis represent an average over five sets of data made up of from 22 to 35 profiles in each set spread over a time span of 10 to 20 days with from 13 to 24 profiles occuring in a basic 48 hours for each set. A distinct peak at a time of 3 hours (corresponding to a wave period of 6 hours) was found in the density, temperature, and pressure (not shown) structure functions. This indicates a preferred gravity wave period of 6 hours during the time from which data were available. No corresponding peak at 3 hours in the structure function of the residual winds was found. The time structure functions at one hour are definitely smaller than those at subsequent hours and can be taken as an indication of the upper limit ε of the contribution from error and small scale turbulence. This rms upper limit ε is related to the structure function at one hour by $\varepsilon = (D(1)/2)^{1/2}$ (cf. equation 17). This relation results in the following estimate for the upper limits of error in the 45 - 65 km height range: 1% for pressure and density, 0.8% for temperature ($\simeq 2^{o}K$), and 3.5 to 4.7 m/s for winds. These estimates are only slightly smaller than those computed by Avera and Miers[8] for this height region. Their estimates were $2.6^{o}K$ for temperature and 6.5 m/s for winds.

The daily difference structure functions in Figure 1 are reasonably continuous with the structure functions of the tidal residuals considering the smaller amount of data available for tidal analysis and the large amount of data in the daily differences. The daily differences in Figure 1 are aver-

aged over three MRN sites (Ascension Island, Cape Kennedy, and Fort Greely) and over altitudes from 45 to 65 km with data from 1964 through 1969. The daily difference magnitudes definitely increase with time separation and it appears that the daily differences at one day separation may be used as a reasonable estimate of the gravity wave contribution because of their general agreement with the large values of the tidal residual structure functions at time scales larger than 5 hours (i.e. periods > 10 hours). The daily difference magnitudes are fairly uniform over the 7 - 15 days time separations and so an average over this interval can reasonably be taken as a measure of the combined gravity wave and planetary wave (up to 30 day period) contributions.

Planetary wave magnitudes were extracted from the 7 - 15 day time separation data for each of the three MRN sites mentioned above by the method described by equation (19), except that instead of one daily difference at large day number n, an average of the daily differences between 7 and 15 days was used. The results are presented in Figure 2. Primary contributions to the planetary wave magnitudes of Figure 2 would come from planetary waves in the period range 14 - 30 days. Data points represent averages over 10 km altitude sections centered about the point. The eastward planetary wave wind component magnitude is larger than the northward component magnitude except at the high latitude site. Significant latitude variation in the 25 to 65 km altitude region was found. A steady increase in planetary wave magnitude with increasing latitude was observed for the pressure, density, temperature, and northward velocity component. The eastward component was reasonably similar at all latitudes. Table 1 gives the names and geographical locations of the MRN sites. Comparison of these results with those obtained by harmonic
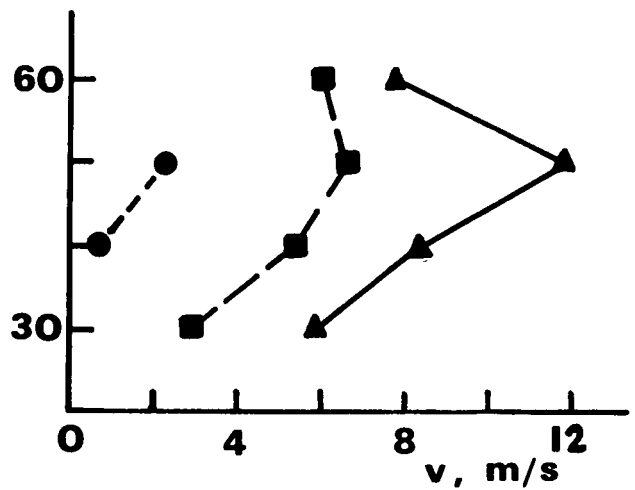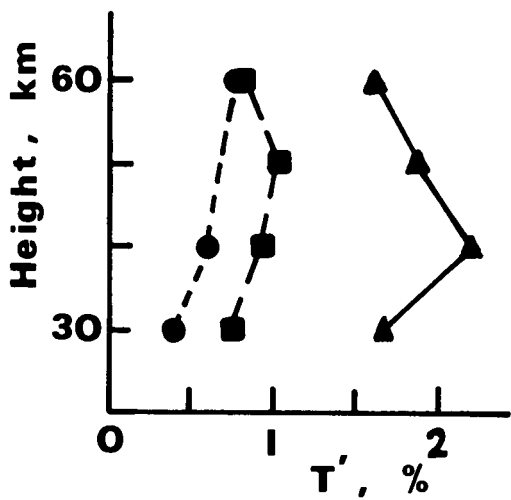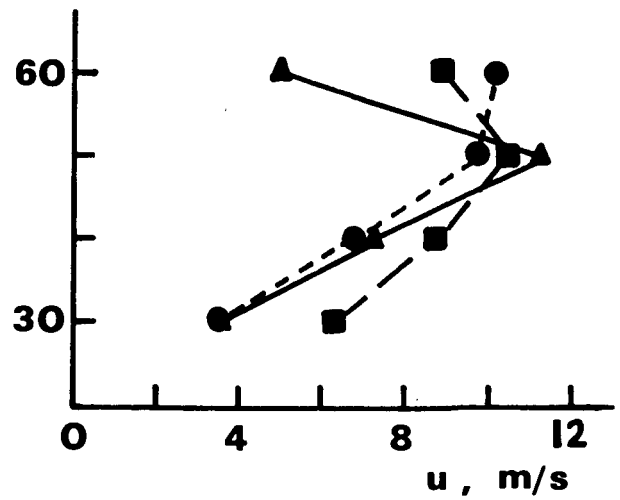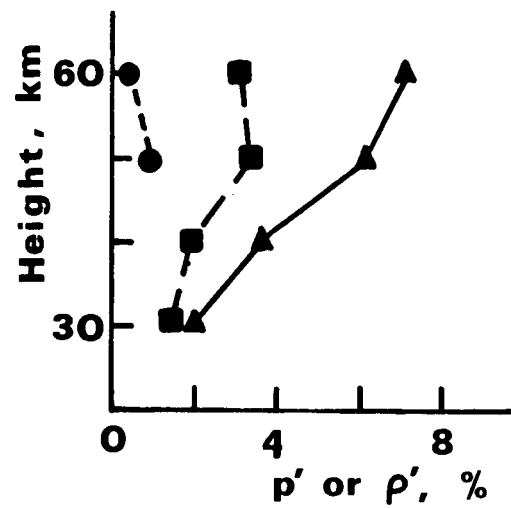
Figure 2. Height and latitude variation of the traveling planetary scale wave component. The solid dots are Ascension Island data, the squares are Cape Kennedy, and the triangles are Fort Greely data.

18

TABLE 1. MRN SITE LOCATIONS

Site Name	Latitude	Longitude
Ascension Island, A.F.B.	7° 59' S	14° 25' W
Fort Sherman, Canal Zone	9° 20' N	79° 59' W
Barking Sands, Hawaii	22° 02' N	159° 47' W
Cape Kennedy, Florida	28° 27' N	80° 32' W
White Sands, New Mexico	32° 23' N	106° 29' W
Point Mugu, California	34° 23' N	119° 07' W
Fort Churchill, Canada	58° 44' N	93° 49' W
Fort Greely, Alaska	64° 00' N	145° 44' W

analysis are presented in Section 6.

Above 65 km there were insufficient data for analysis of separate sites and so all data were combined for averaging. In the 65 - 85 km region and above it was found that the daily differences at 7 - 15 days time separation were not significantly larger than one day differences, which indicates no measurable propagation of planetary waves to this altitude range. However, as discussed more fully in the next section, there is evidence for propagation of selected wavelengths of planetary waves into the 65 - 85 km region.

Gravity Wave Statistics. In the previous report[1] it was shown that probability distributions of the gravity wave fluctuations could be determined from the distribution of daily differences. In the light of the discovery of significant planetary wave contributions in the 25 - 65 km region, only daily differences over one day should be used to determine the gravity wave distributions. Details were given in the earlier report on the methods of determining the distributions and the corrections applied. Figure 3 shows an example of the measured distribution of gravity wave perturbations determined from daily differences over one day. Values expected from a Gaussian distribution are shown for comparison.

Some properties of importance in the study of the probability distributions of a property x are the mean $\bar{x} = <x>$ and higher moments. The variance is given by $\sigma^2 = <(x - \bar{x})^2>$ the skewness is $\alpha = <(x - \bar{x})^3>/\sigma^3$ and the kurtosis is $\beta = <(x - \bar{x})^4>/\sigma^4$. Table 2 shows the mean values of the gravity wave statistical parameters in the 50 to 80 km altitude region as determined from distributions of the single day daily differences. In Table 2, as elsewhere u is the eastward velocity component and v is the northward component. In the 45 - 65 km range the kurtosis values β are all larger than the expected Gaussian distribution value of 3, whereas in the 65 - 85 km

20

region all of the β values except for the temperature β are less than 3. These revised values of kurtosis are similar to, though slightly different from, the previous results[1] in this height range. There are no changes from the higher altitude values previously reported.

An analysis was performed to determine if the high β values in the 45 - 65 km region could be due to intermittent gravity wave disturbance. Let us presume the following situation: A certain fraction γ of the total observations consist only of Gaussian distributed error with standard deviation σ_e. The fraction γ is known as the intermittency. The remaining fraction (1 - γ) of the measurements consist of Gaussian distributed gravity wave perturbations* with standard deviation σ_g superimposed on the background error. Mosley[9] has shown that the kurtosis of the combined set of observations is given by

$$\beta = 3(1 - \gamma H^2)/(1 - \gamma + \gamma H)^2 \tag{29}$$

where the ratio H is $\sigma_e^2/(\sigma_e^2 + \sigma_g^2)$. Equation (29) reduces to β = 3, the Gaussian value, in the limiting cases of no gravity waves (σ_g = 0 or γ = 1) or no error (σ_e = 0 or γ = 0). Figure 4 shows isocontours of β on the H - γ plane. From the error estimates discussed above and the gravity wave magnitude estimates it was concluded that H ≃ 0.2 for pressure and density, H ≃ 0.3 - 0.4 for winds and H ≃ 0.5 for temperature in the 45 - 65 km region. From Figure 4 it is possible that the observed β values for pressure and density (from Table 2) could have been produced by an intermittency factor of 0.7 to 0.9. However, the remaining observed β values (i.e. for temperature and winds) cannot be explained by intermittency.

_____

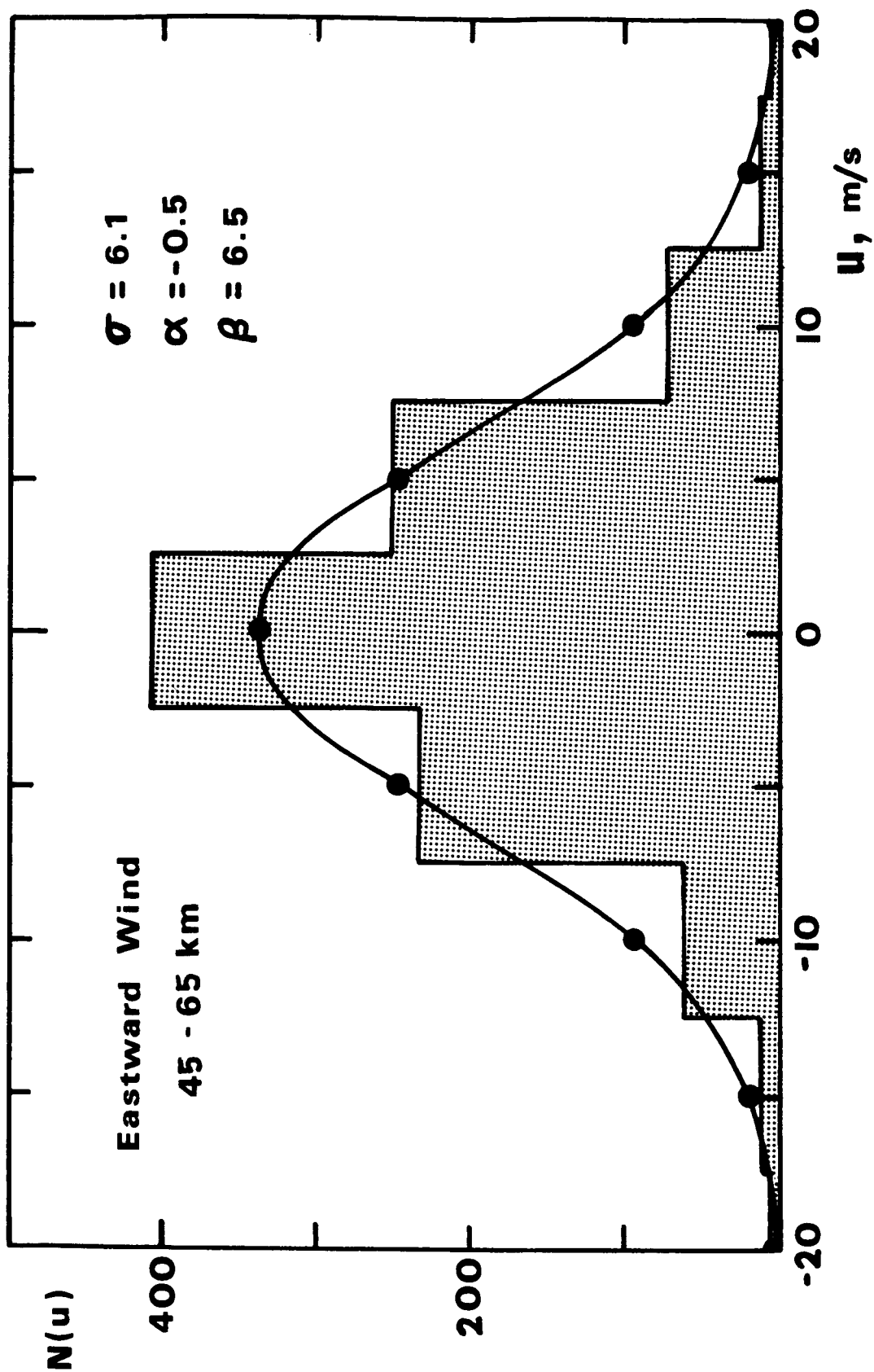* This presumes several superimposed wave modes interacting more-or-less randomly.

Figure 3. Probability distribution of gravity wave eastward wind component in the 45-65 km height region. Shaded histogram gives observed distribution and solid dots show expected values from gaussian distribution of same standard deviation and zero mean.

TABLE 2. Average gravity wave statistics
in the 45 to 85 km region. N is the num-
ber of independent values, α is the skew-
ness and β is the kurtosis.

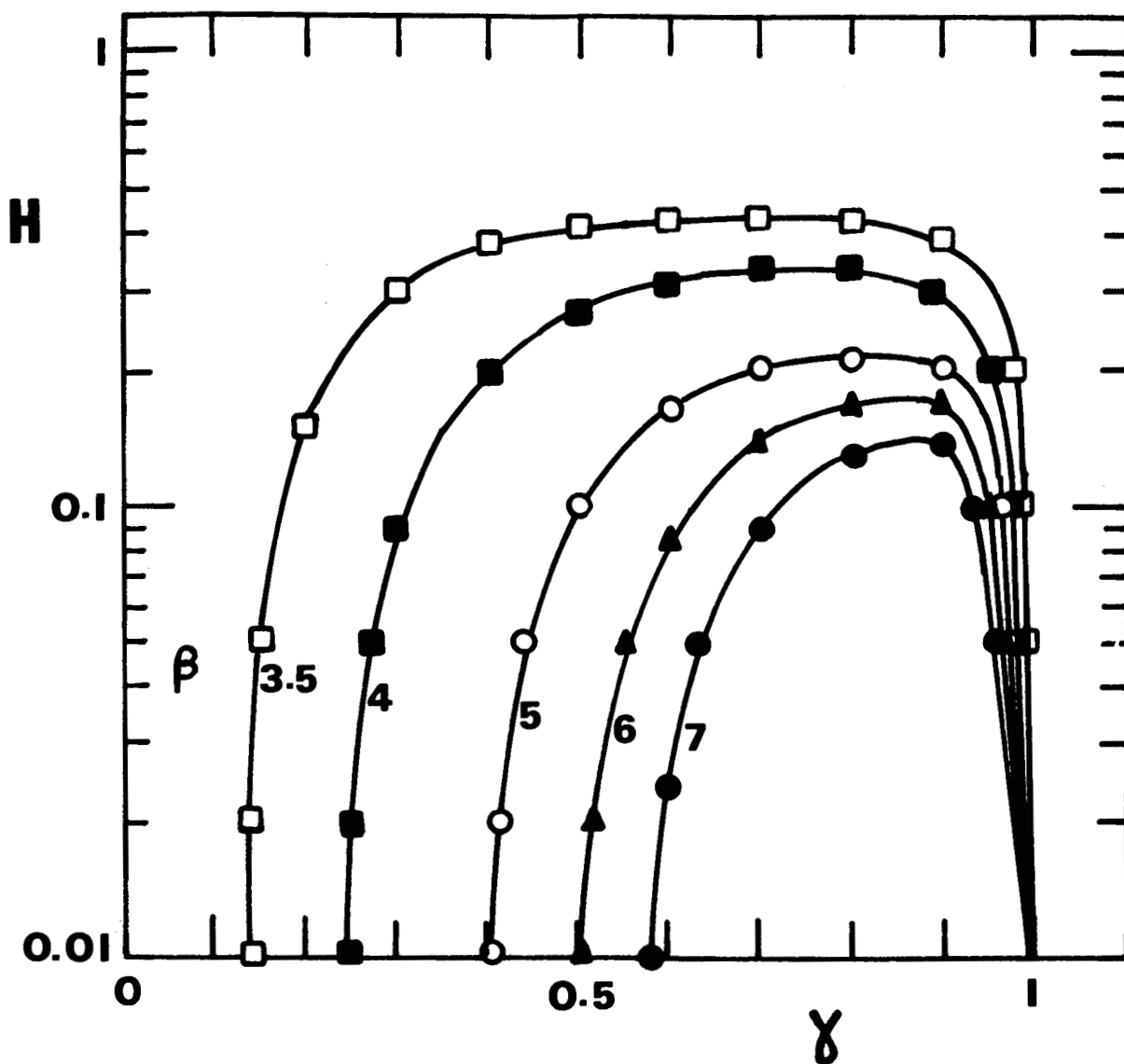|	45 – 65 km			65 – 85 km		
	N	α	β	N	α	β
p	1203	+0.28	6.56	126	+0.35	2.18
ρ	1213	+0.16	5.68	126	+0.55	2.56
T	717	−0.54	15.55	126	−0.23	4.48
u	1934	−0.07	5.69	59	+0.07	2.42
v	2033	−0.08	4.47	59	+0.02	2.29

Figure 4. Values of kurtosis β at various values of
the ratio H and the intermittency γ as determined
from equation (29).

Gravity Wave Magnitudes. The daily differences over one day separat-
ion were used to compute revised gravity wave magnitudes in the 45 - 85 km
region and new values in the 25 - 45 km region. Because planetary scale
waves were not detectable in the 95 - 115 km region[5] the previous data,
determined from averages over 1 - 15 day separation daily differences, were
retained as the best estimates of gravity wave magnitudes above 85 km.

Figure 5 shows the height variation of the measured average gravity
wave magnitude. The data in Figure 5 were obtained from 1964 - 1969 MRN
data one day differences from all eight sites listed in Table 1 plus all
of the other falling sphere, grenade, pitot tube, chemical release, and
satellite data collected. Meteor wind data from Garchy, France[10], Durham,
New Hampshire[11] and Kazan, Russia[12] are shown separately in Figure 5.
These meteor wind results are residual winds after explicit resolution of
the tidal winds by the method of Groves[13]. The error bars in Figure 5
were computed by the method outlined in Appendix A.

The meteor wind results agree qualitatively although not in detail
with the average results from the other data. However, it should be noted
that the meteor results from Garchy and Durham were each determined from
one set of measurements over a few days whereas the other results were
obtained from several profile pairs from times spread over several years.

The two gravity wave velocity components appear to be isotropic over
the full altitude extent of Figure 5 with the possible exception of a
slight predominance of the eastward component near 140 km.

Linearized gravity wave theory[14] with no dissipation or reflection
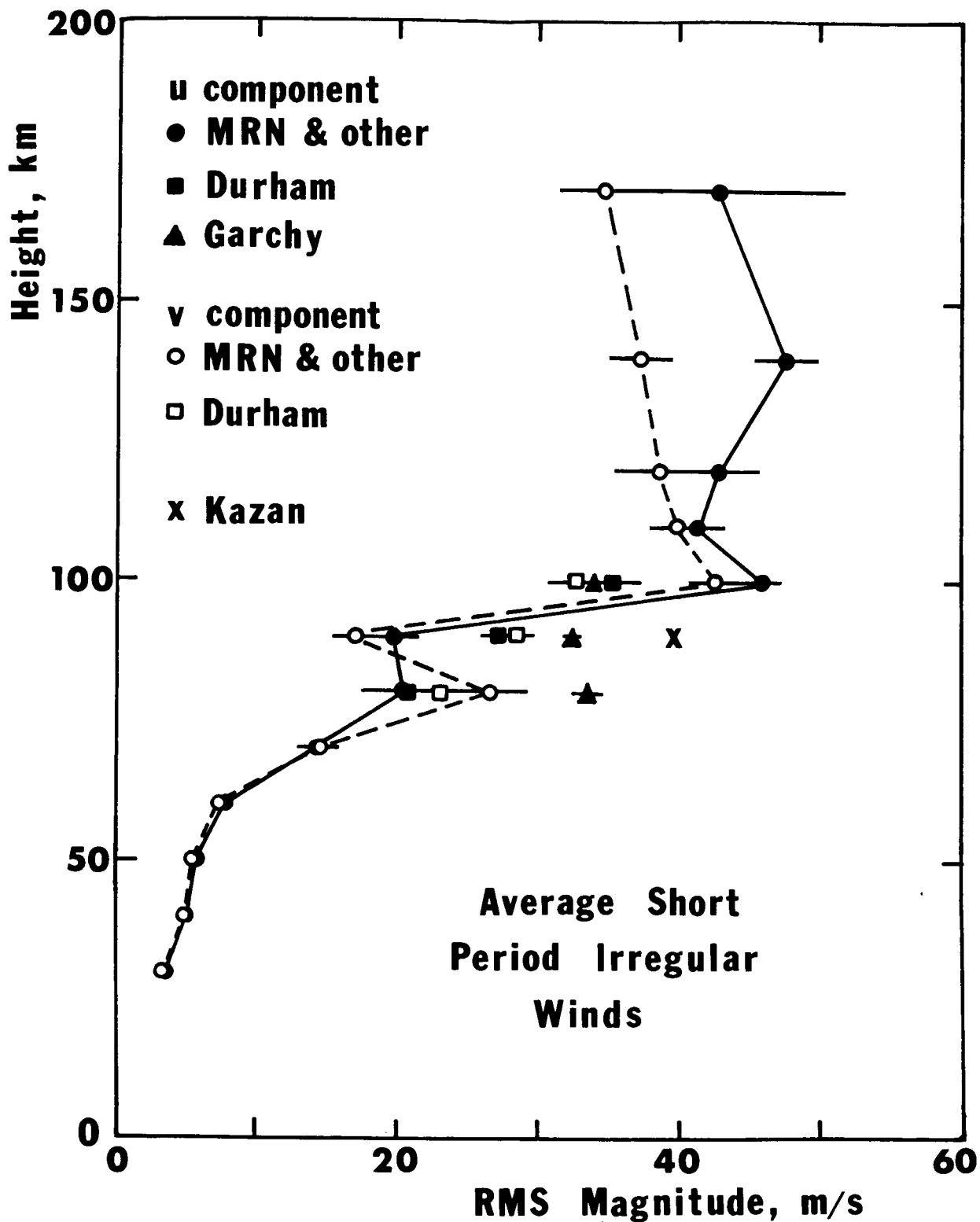predicts that the gravity wave kinetic energy density $\rho_o <u^2 + v^2>$ remains

Figure 5. Height variation of the magnitude of the gravity wave wind components. The eastward component is u and the northward component is v.

constant with height. However, Figure 6 shows that considerable dissipat-
ion and/or reflection takes place, on the average, throughout most of the
atmosphere. One exception is the 55 to 75 km height region, which corres-
ponds to the decreasing temperature gradient of the atmosphere, a region
where gravity wave reflection is not expected. At 90 km in Figure 6 the
solid dot represents the MRN and other data and the open circle represents
an average value including the meteor wind data. Between 75 and 135 km the
average gravity wave kinetic energy density varies with height as

$$\rho_o <u^2 + v^2> \propto \exp(-z/z_o) \tag{30}$$

where the "scale height" value z_o is 7.8 km, in good agreement with the
value determined by Kochanski[15] in the upper portion of this altitude
range. Between 25 and 55 km the value for z_o is 9.4 km. Extrapolation
of $\rho_o <u^2 + v^2>$ to 10 km indicates that jet stream level perturbations of
about 3 m/s would be required to maintain the same rate of dissipation or
reflective loss between 10 and 30 km as that observed between 30 and 50 km.
If tropospheric propagation from the surface to 10 km is assumed to be at
constant energy, analogous to the mesospheric propagation, then surface
perturbations of about 1.8 m/s could maintain the dissipation or reflect-
ive loss of the extrapolated curve. The change of slope above 135 km is
due to a change in the density variation at this altitude while the gravity
wave wind magnitude remains approximately constant with height.

The height variation of the irregular pressure, density, and temper-
ature is shown in Figure 7. The data are expressed as variation relative
to the mean atmospheric parameters. Error bars in Figure 7 were also com-
puted by the method outlined in Appendix A.
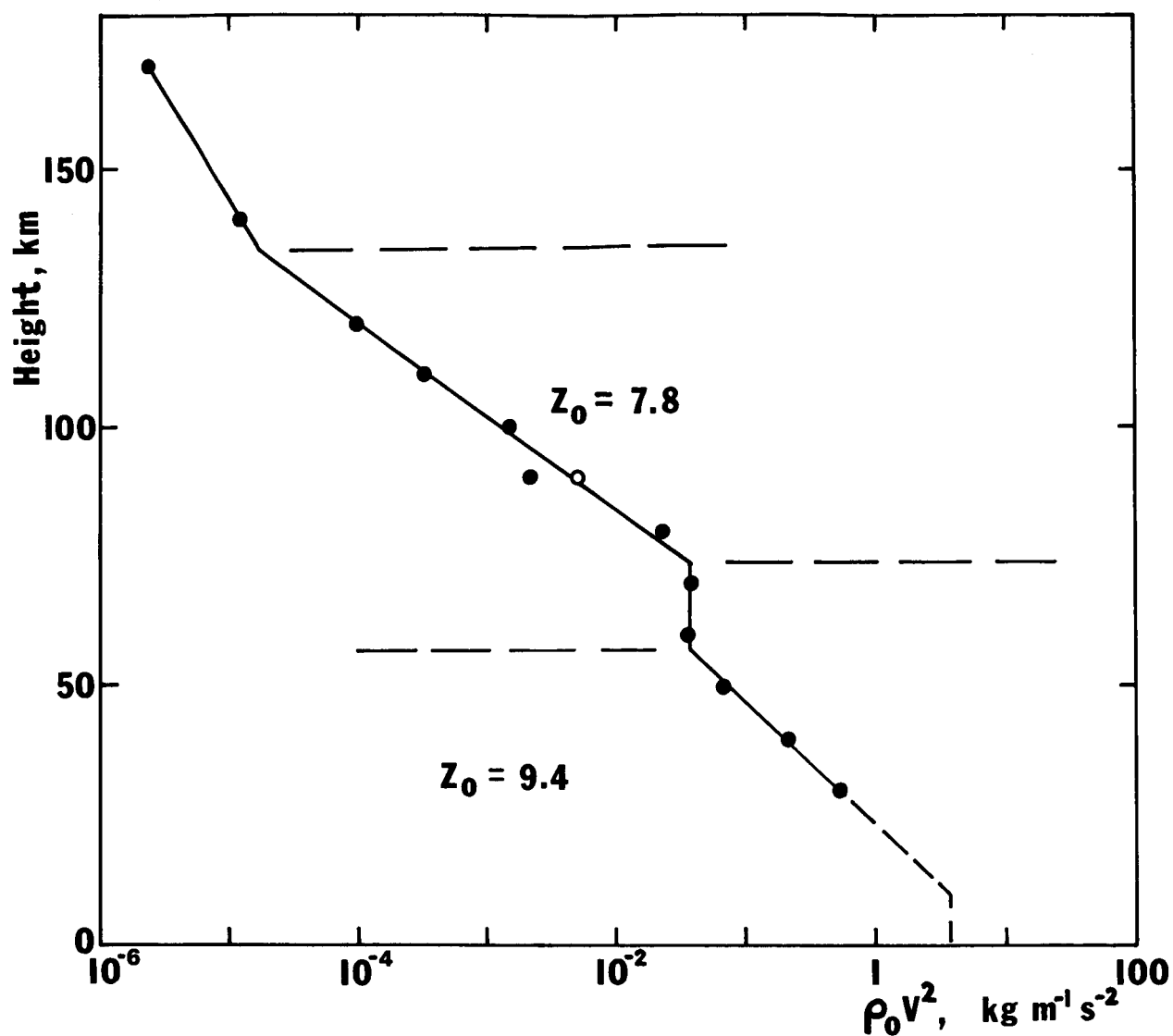
Figure 6. Height variation of the kinetic energy density of the gravity wave winds. Z_O values are energy "scale height" values for equation (30). The solid dots are the MRN and other data. The open circle at 90 km is an average value including the meteor wind data.
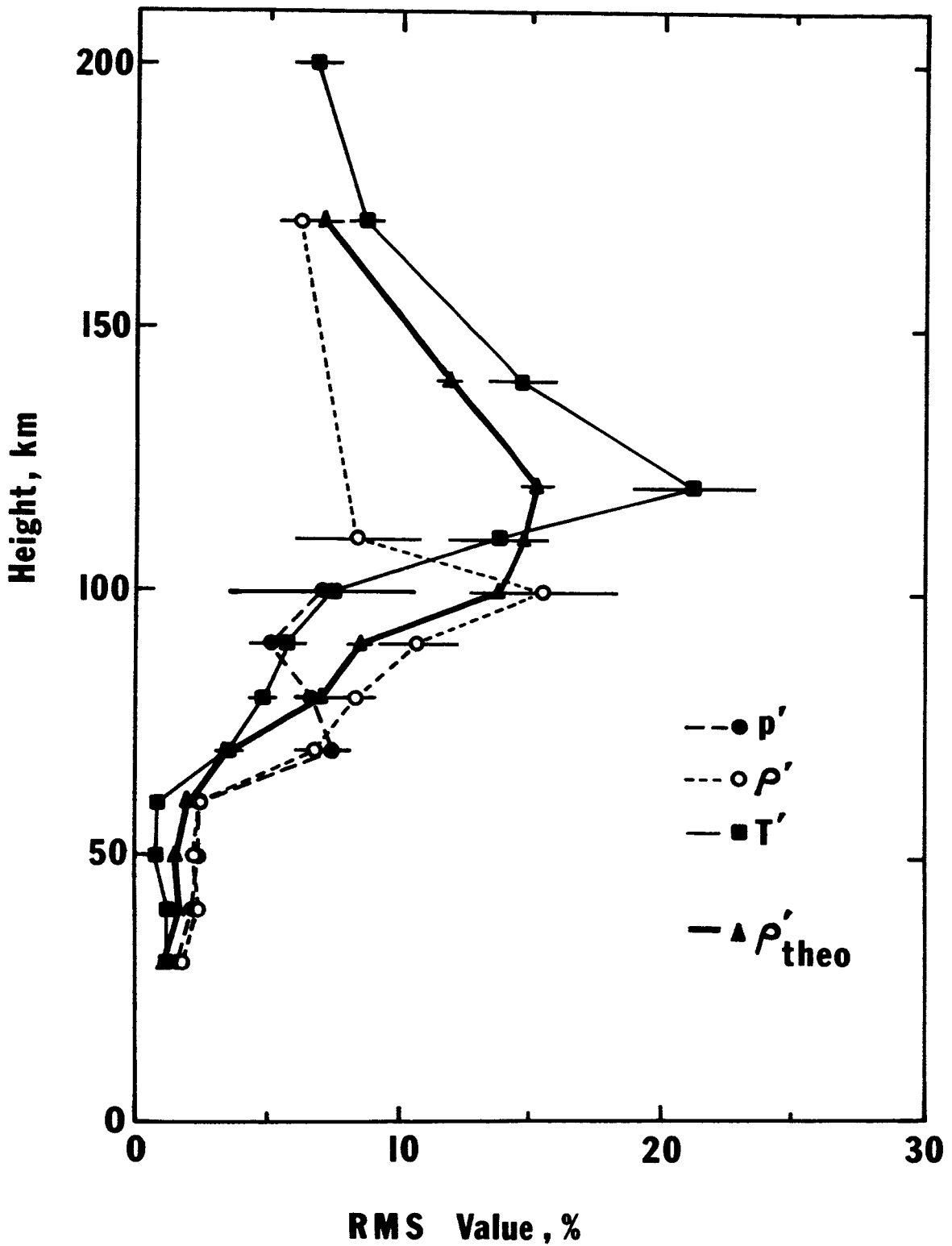
Figure 7. Height variation of the magnitude of the relative pressure p'/p_o density ρ'/ρ_o, and temperature T'/T_o due to gravity waves, and the theoretical ρ'/ρ_o curve of Miller[17], equation (33), based on observed gravity wave winds from Figure 6.

Figure 7 shows that the relative temperature variation magnitude between 40 and 70 km is significantly smaller than for the relative pressure or density, which are about equal. Between 80 and 100 km the relative pressure and temperature variation magnitudes become about equal and smaller than the relative density variations. Above 100 km the relative density variations become smaller than those for the relative temperature.

At first one might think that the Boussinesq approximation should apply to the pressure, density, and temperature variations and hence that the relative pressure variations should be much smaller than the relative density and temperature. However, as shown by Dutton and Fichtl[16], for motions of vertical scale not small compared to the scale height, the magnitudes of all three parameters are comparable. It will be shown later that the vertical scales are comparable with the scale height. Therefore, the relative values of the irregular thermodynamic parameters are related by

$$p'/p_o = \rho'/\rho_o + T'/T_o \tag{31}$$

and in the mean square they would be related by

$$<(p'/p_o)^2> = <(\rho'/\rho_o)^2> + <(T'/T_o)^2> + 2<(\rho'/\rho_o)(T'/T_o)> \tag{32}$$

where the last term is basically the correlation between the density and temperature variations, which in the case of a single component wave train would be dependent on the relative phase between the density and temperature wave variation. The changes discussed above in the relative magnitudes of the thermodynamic variables of Figure 7 therefore indicate a changing phase relationship with height. The changing phase relationship could be due to

nonlinear intermodal interactions or to selective modal absorption of a complex gravity wave field. In either case it would be difficult to justify the changing relative magnitudes with the assumption of a single mode gravity wave field.

A comparison of the height variation of the irregular winds and irregular density, also shown in Figure 7 gives good agreement with a theory developed by Miller[17], which predicts relative density variations proportional to rms velocity variation by a factor which varies with height. The theoretical values of ρ'/ρ_o are related to the mean square irregular winds by the formula

$$\left|\rho'/\rho_o\right| = \left\{\left[(\gamma - 1)/c^2 + (1/gT_o)\ dT_o/dz\right] <u^2 + v^2>\right\}^{1/2} \tag{33}$$

This theory is applicable in the strict sense only to single mode gravity waves. The U.S. Standard Atmosphere of 1962 was used to evaluate the speed of sound c, the acceleration of gravity g, the temperature T_o and its height gradient dT_o/dz. The ratio of specific heats γ was assumed to be constant at a value of 1.4. The agreement between the observed ρ'/ρ_o variation and that predicted by the theoretical formula is remarkably good, considering the uncertainties introduced by the use of standard atmosphere values and the application to what is apparently a multi-mode gravity wave field. However, it does appear from the results shown in Figure 7 that the theoretical formula corresponds more nearly with the magnitude of the irregular temperature T'/T_o than the density ρ'/ρ_o. This discrepancy would have been improved considerably, however, if the density value at 110 km had been somewhat larger than the value actually observed.

The three sites, Ascension Island, Cape Kennedy, and Fort Greely had

31

sufficient data for daily differences over one day separation so that separate evaluations could be made for these sites. Figure 8 shows the altitude variation of the rms gravity wave magnitudes at these locations. There is no apparent system which describes the variation with latitude at all altitudes, although at many heights the magnitudes of winds and temperature fluctuations are smaller for the Fort Greely site. The large increase in wind magnitude between 50 and 60 km is compatible with the constant kinetic energy in this region, as discussed above.

The large amplitude of daily differences at the White Sands site previously reported[1] were found to be associated with the daily differences over large day separations and not with the single day daily differences. Hence, these large amplitudes of wind variation are to be associated with the planetary scale components rather than the gravity wave components.
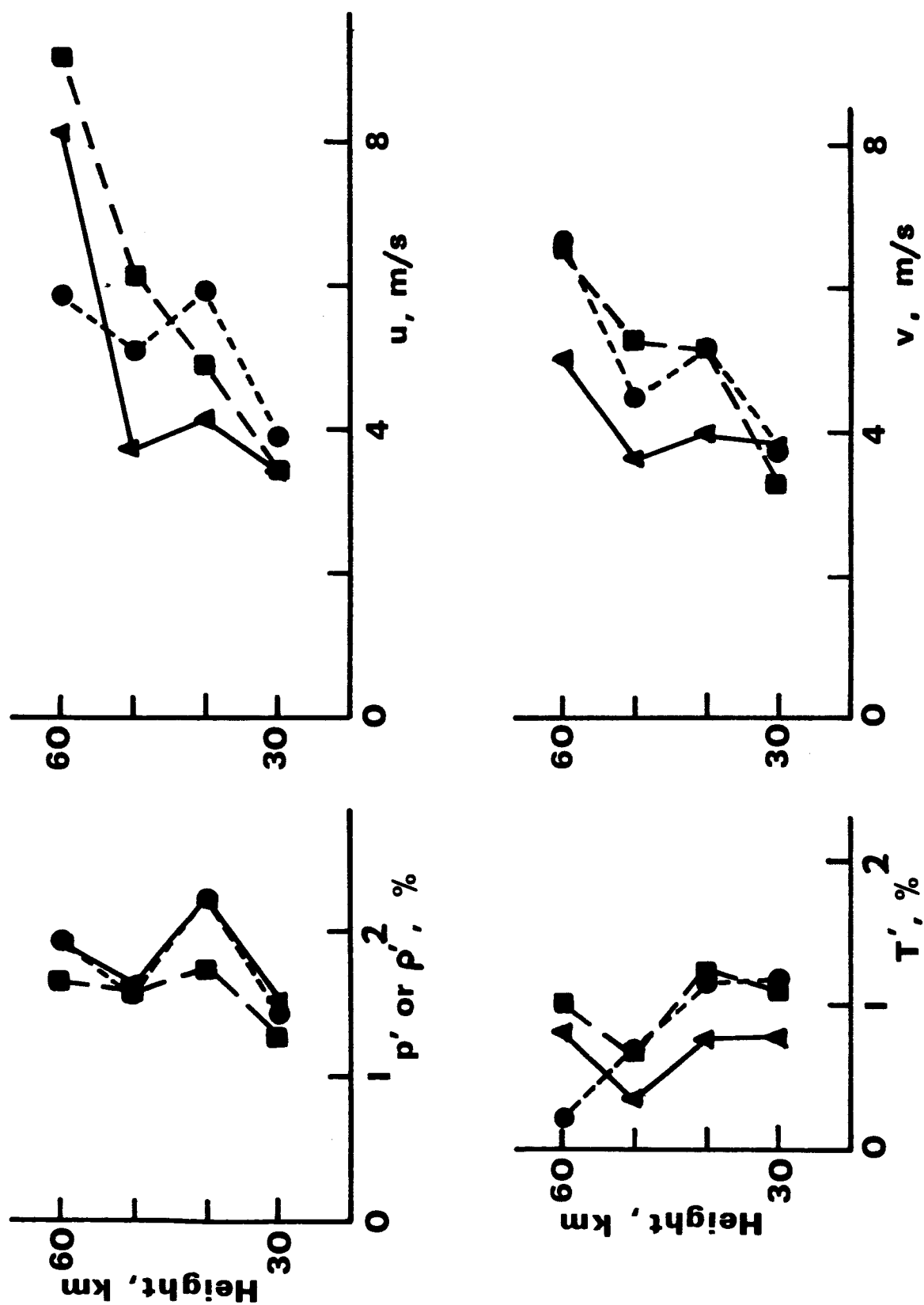
32

Figure 8. Height and latitude variation of the gravity wave component.
Ascension Island data is shown by the solid dots, Cape Kennedy by the squares,
and Fort Greely by the triangles.

33

4. SCALES OF GRAVITY WAVE VARIATION

Vertical Scales. The vertical structure function of a parameter $F(z)$ is given by

$$D_F(\zeta) = \langle [F(z + \zeta) - F(z)]^2 \rangle$$

and, as shown in equation (23), the vertical structure function of the gravity wave components can be estimated from one half the vertical structure function of the daily differences ΔF_1 taken over one day separation. Also, as shown by equation (25) the vertical structure function of the planetary wave components can be evaluated from the difference between the vertical structure functions of large day daily differences ΔF_n and single day daily differences ΔF_1.

Vertical scales of the gravity wave components can be estimated from the single day daily difference vertical structure functions by the technique discussed in Section 2. Figure 9 shows measured average vertical structure functions of gravity wave winds and temperature variations in the 45 - 65 km height range. Solid curves are fit through the data as determined from the exponential correlation functions suggested in Section 8.

Figure 9 also shows the average vertical structure function of the large day daily differences. The difference in the two curves would be the structure function of the planetary scale waves alone. It appears that there is some contribution to the structure functions from planetary scale waves of vertical wavelengths in the 10 to 30 km range, somewhat larger than planetary scale vertical wavelengths at lower altitudes. However, as the size of the error bars indicate, the firm conclusions which can be made on the vertical structure of planetary waves are somewhat limited. The discrete vertical

34

Figure 9. Vertical structure function of the gravity wave component in the 45-65 km height range determined from the single day daily differences (solid dots) and the vertical structure function of the 7-15 day daily differences (open circles). Curves through the data points are computed from $D(\Delta z) = 2\sigma^2 [1 - \rho(\Delta z)]$ where the correlations are the exponential functions discussed in Section 8.

wavelength reported earlier[1] which appeared in data from some, but not all, sites seems to be associated with the large day daily differences, i.e. planetary scale waves, rather than the gravity wave components.

The amount of data in the 65-85 km height range for vertical structure analysis was somewhat limited. Nevertheless some structure function results were obtained and these are shown in Figure 10. The vertical structure functions of the 10-12 day daily differences (i.e. up to 24 days period) are distinctly different from the one day differences and seem to indicate a preferred vertical wave length for the planetary waves of 20 km (structure function maximum at 10 km). However, the fact that the mean square daily differences were not significantly larger than the mean square single day differences, is taken to indicate a rather selective or sporadic propagation of these planetary waves into the 65-85 km region.

Vertical structure functions above 85 km were not revised and remain unchanged from the results presented earlier[1].

Horizontal Scales: There are no useable data available from which to determine horizontal structure of pressure, density, or temperature. The horizontal structure function of the winds in the 50 to 65 km region was slightly revised and is shown in Figure 11 (with a plotting error of the original graph corrected). Also shown in Figure 11 is a plot of the horizontal structure function of winds in the 80-140 km height range. The solid curves fitted through the data in Figure 11 were evaluated from the engineering approximation functions discussed in Section 8, using σ values determined from the daily difference analysis.
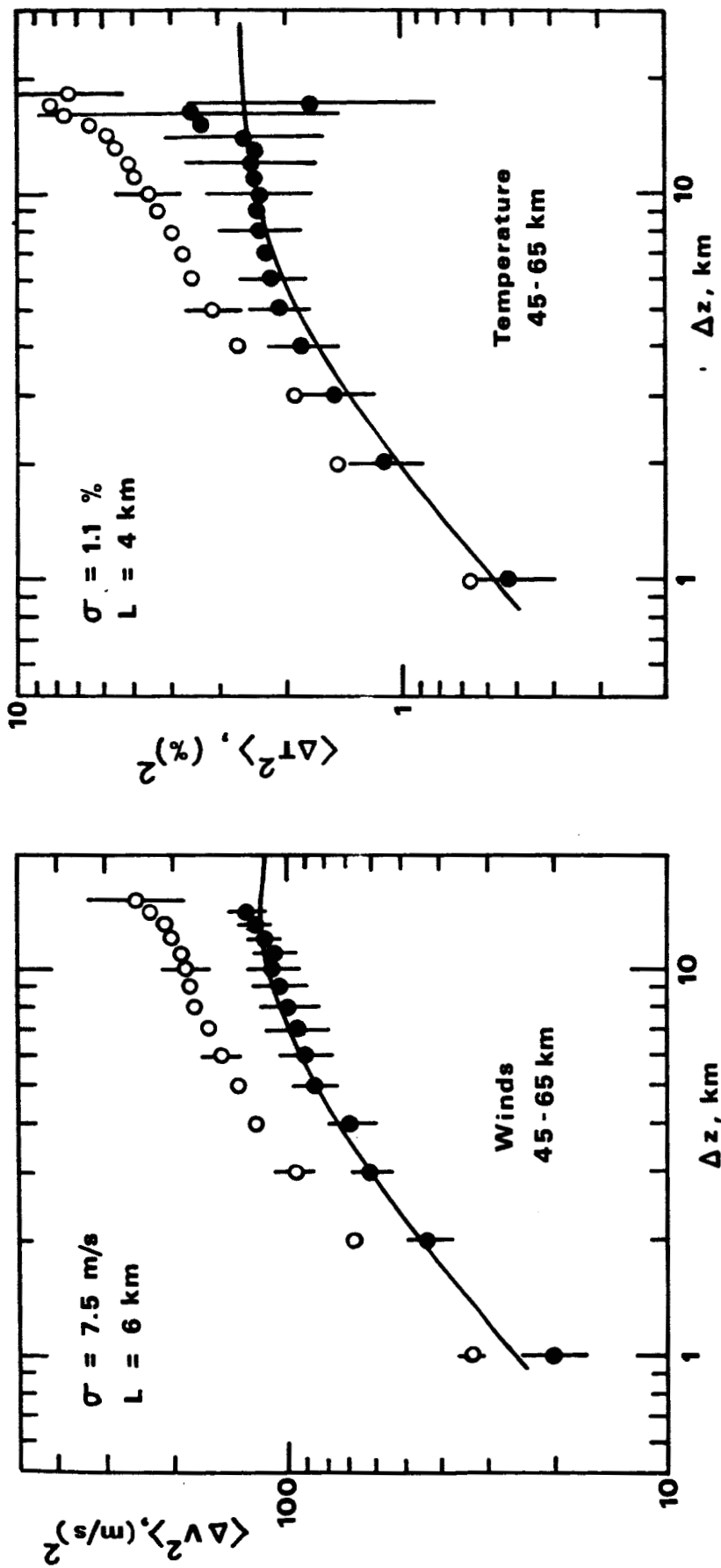
36
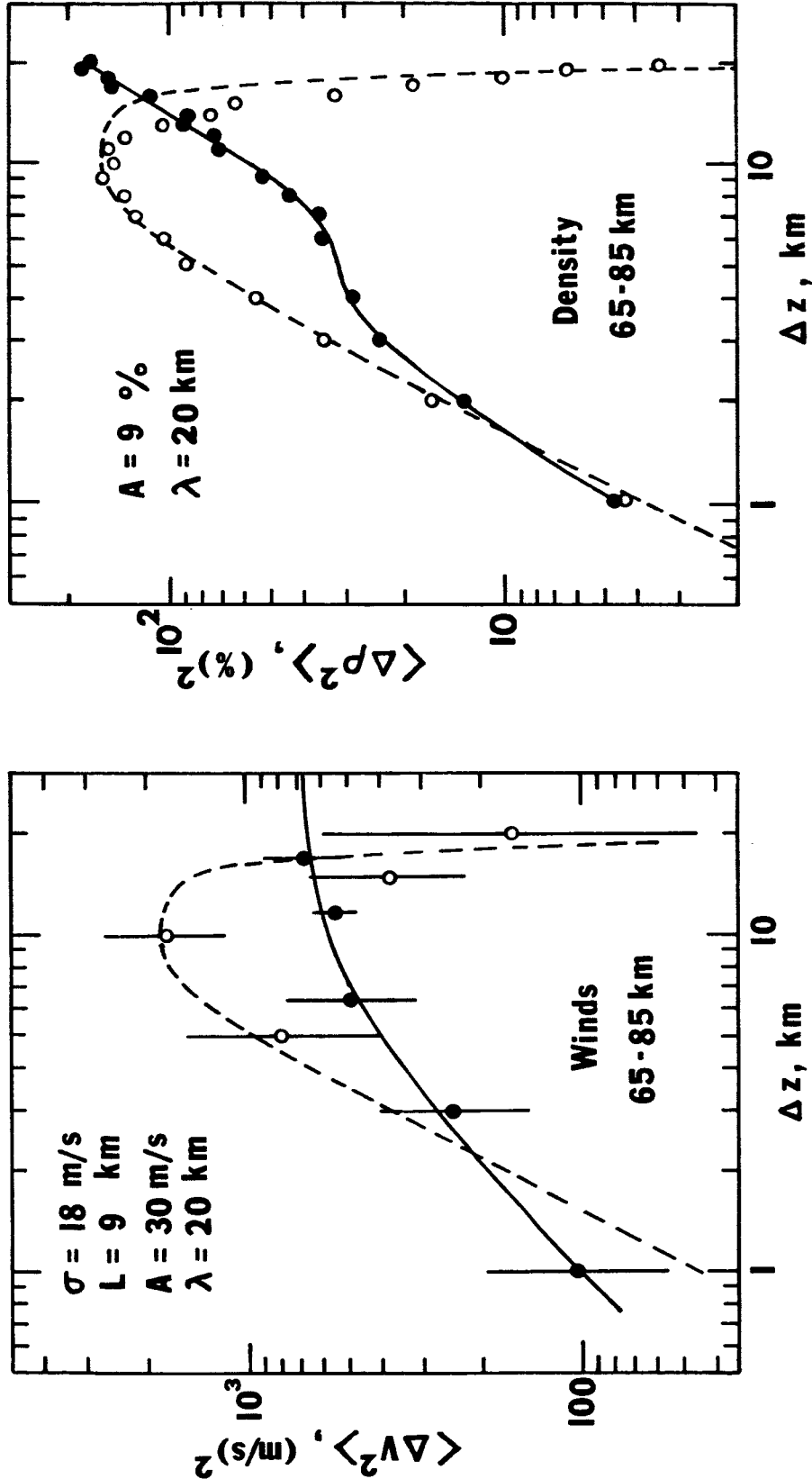
Figure 10. Vertical structure function of the gravity wave component in the 65-85 km height range determined from the single day daily differences (solid dots) and the vertical structure function of the 10-12 day daily differences (open circles). The solid curve through the gravity wave winds was determined as in Figure 9. The solid curve through the gravity wave density data is an empirical fit to the data points. Dashed curves are single wave length formulas $D(\Delta z) = A^2 [1 - \cos(2\pi \ \Delta z/\lambda)]$ (see Section 2).

37
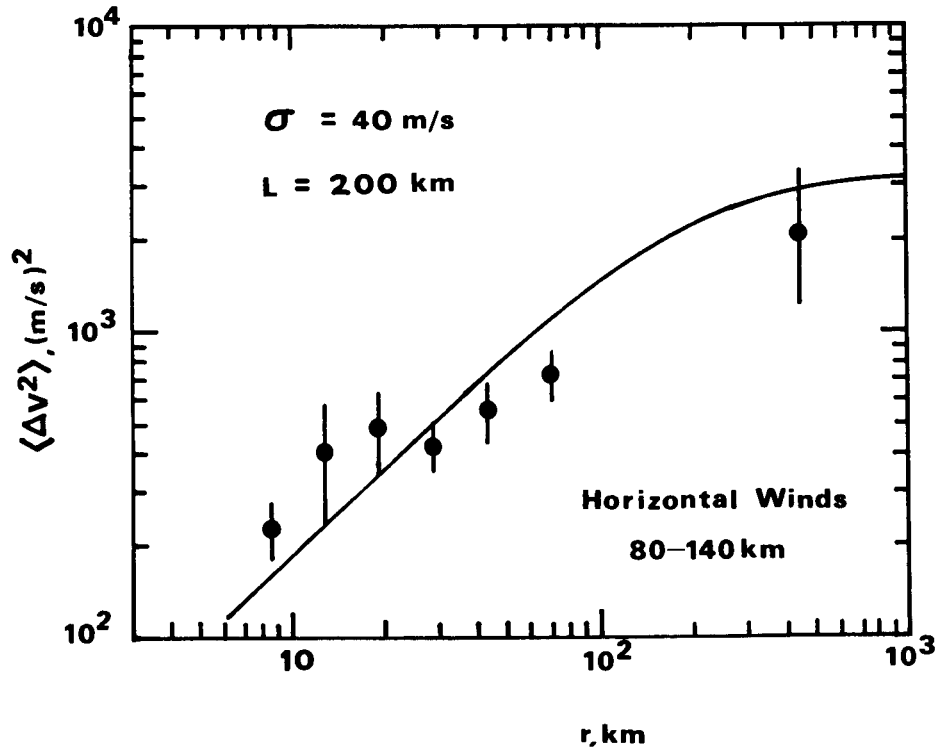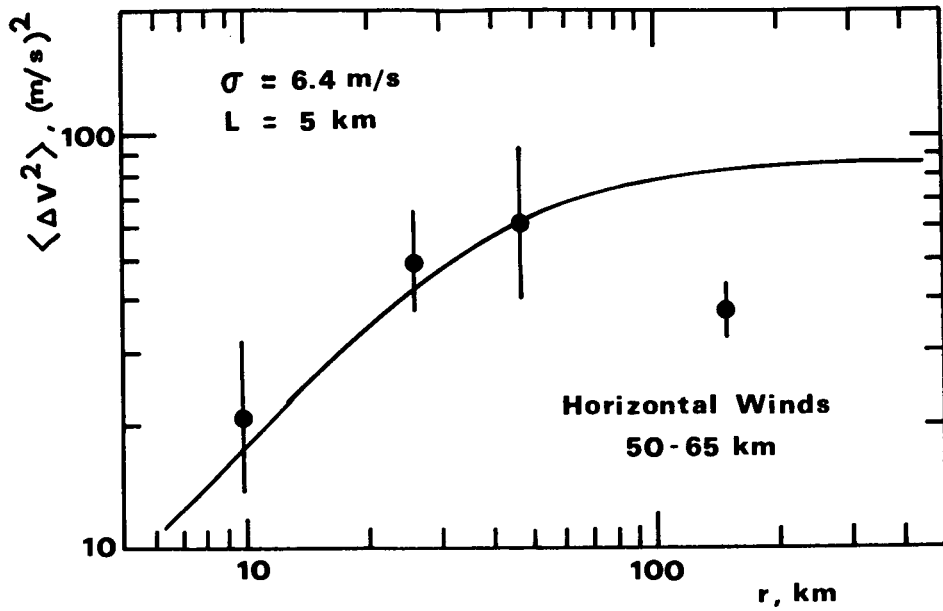
Figure 11. Horizontal structure function of winds in the 50 to 140 height region. Curves through the data points are determined from $D(r) = 2\sigma^2[1 - \rho(r)]$ with $\rho(r)$ given by $\rho(r) = [R_{11}(r_1) + R_{22}(r_1)]/2$ and the correlations R_{11} and R_{22} given by equations (40) and (41) in Section 8.

5. TIDAL HARMONIC ANALYSIS

Tidal harmonic analyses have been performed previously by Justus and Woodrum[1] on nine different sets of MRN data as an interim step to obtaining profiles of irregular winds, temperature, pressure and density. However, the analyses were performed on the raw data which were not smoothed or corrected for solar radiation. Also, the length of the data records included only a basic 24-to-48 hours interval and did not take advantage of any additional data at scattered times around this basic interval. Thus, much better harmonic analysis results could be obtained if the above problems were corrected. Then, better profiles of the irregular components would be obtained, which, in turn, would give better estimates of gravity wave amplitudes by means of the time structure function. The revised time structure function data were shown in Figure 1 for comparison with daily difference analysis results.

Smoothing and Solar Radiation Correction. First, the temperature data were corrected for solar radiation by a procedure given by Hoxit and Henry[18]. This procedure was valid only for certain types of temperature sensors. Hence, all data sets which used sensors other than these particular types were eliminated from the analysis. It was found that five good data sets were left: one set from Ascension Island, A.F.B. around April 12, 1966; three sets from White Sands, New Mexico, around February 7, 1964, November 22, 1964 and July 1, 1965; and one set from Fort Churchill, Canada, around September 8, 1966. After the temperature data were corrected, the pressure and density data were recalculated from the hydrostatic equilibrium equation and the equation of state.

39

Then, all the wind and thermodynamic data were smoothd by the use of a polynomial smoothing function over a height interval of five kilometers.

Extended Time Interval. Preliminary error analysis by Woodrum and Justus[19] indicated that significant differences in evaluated tidal parameters may result if a data record of longer than 24 - 48 hours is used compared to results computed from a 24 - 48 hours data record. Further investigations have substantiated these earlier results. A preliminary analysis of errors was made by the following procedure: Thirty sets of fictitious data were created by superimposing a random error on smooth tidal data which included the periods of 24 and 12 hours as given by the following equation.

$$Y(t) = 10 \sin (\frac{2\pi t}{24}) + 5 \sin (\frac{2\pi t}{12} + \theta) + 12R \qquad (34)$$

where R is a random number between -1 and 1. The amplitude of the random component in equation (34) is representative of the fluctuations produced by gravity waves and traveling planetary scale waves of a few days period, as determined in Section 3.

Harmonic analyses on the 30 data sets were performed and standard deviations of the amplitudes and phases were found. Then, the time length of each data set was reduced and the harmonic analysis was repeated. This process gives the standard deviation as a function of the time length of the data sets as shown in Figure 12 and 13. These figures show results of two analyses for diurnal and semidiurnal oscillations where the data sets first had values at every hour and then had values only for every third hour. It is seen from the figures that the errors seem to be rather small unless the time length of the data set is less than about three days. The basic time length of the
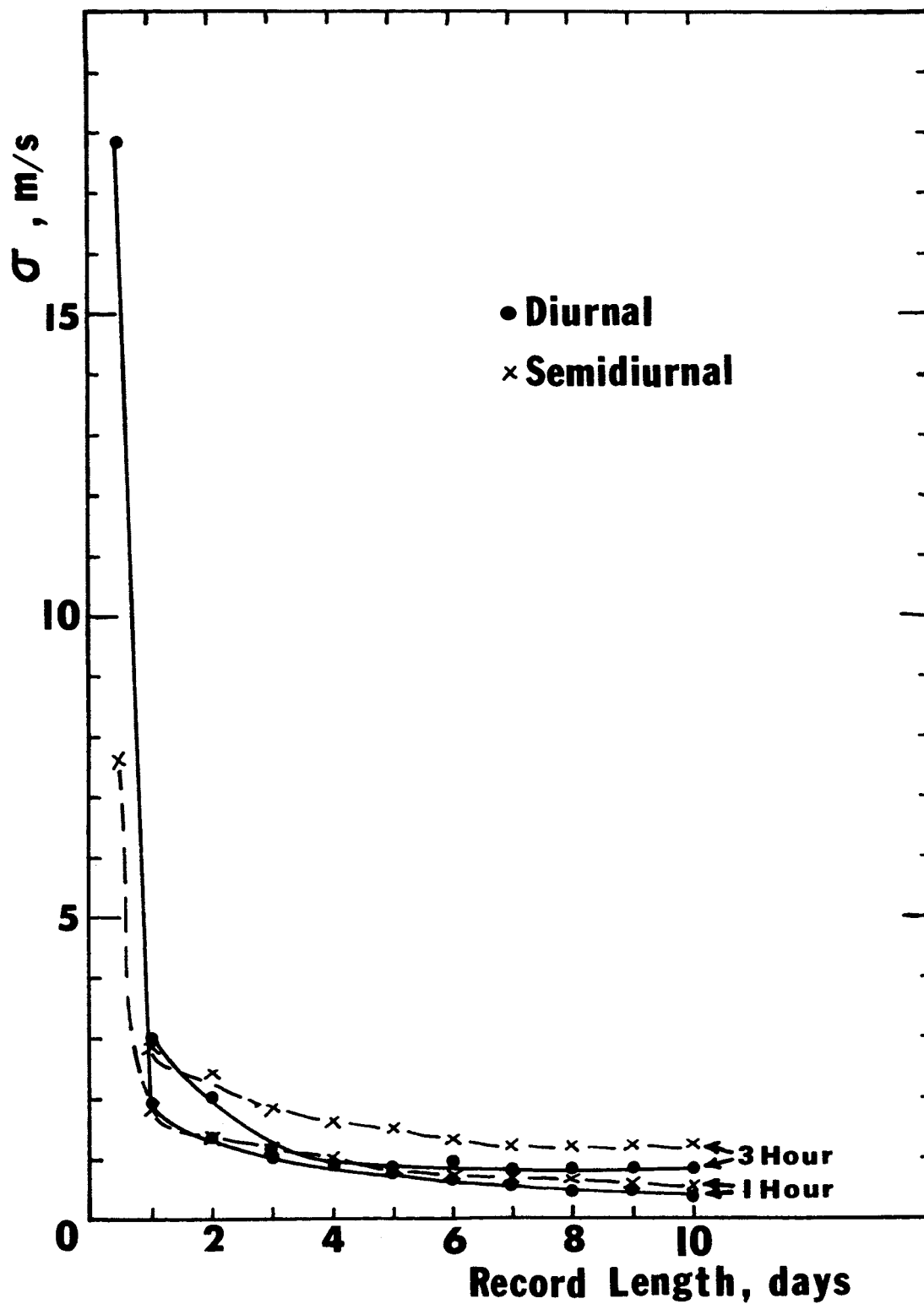
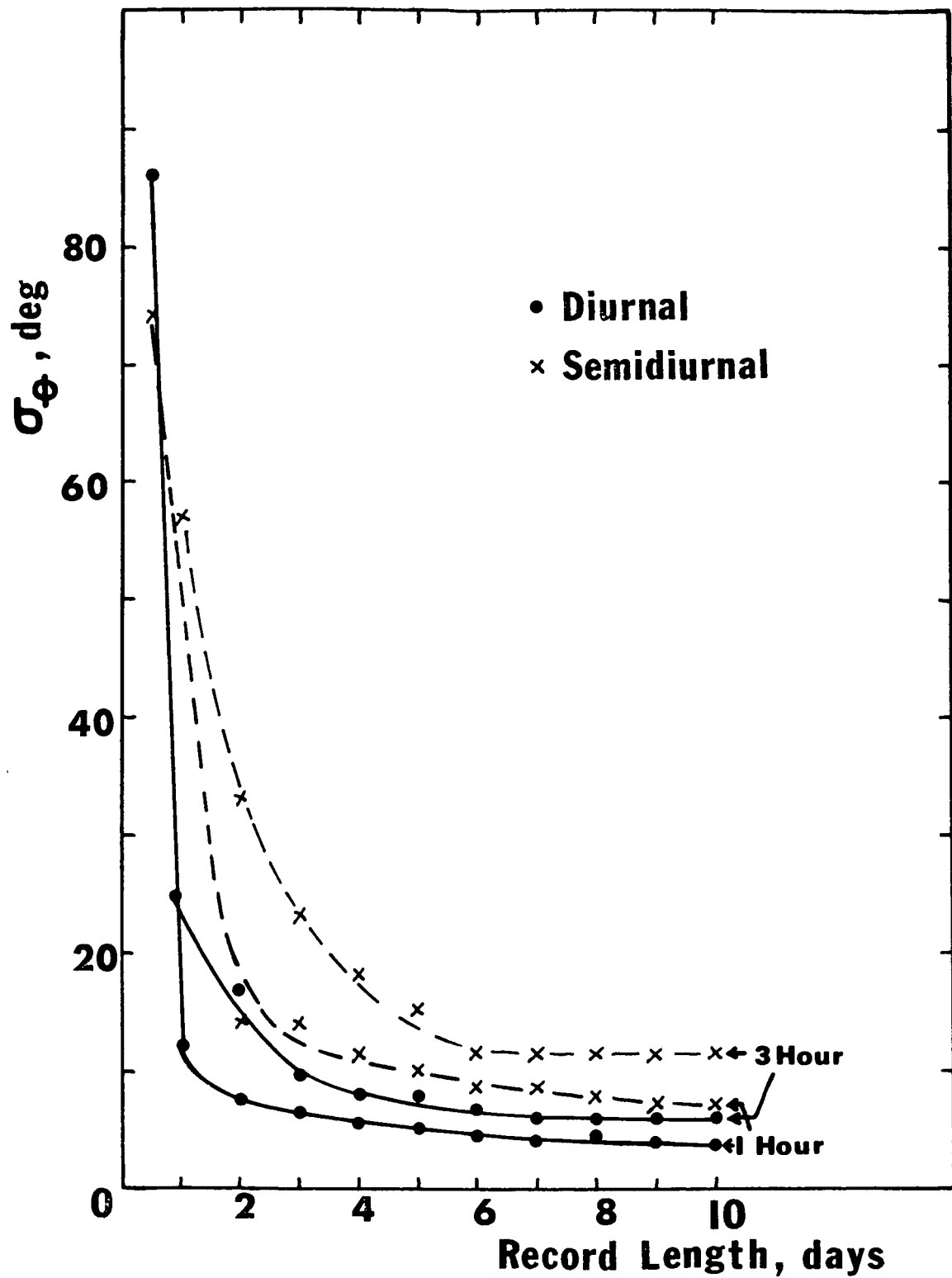Figure 12. Amplitude Error Analysis of Simulated Data.

Figure 13. Phase Error Analysis of Simulated Data.

42

observed MRN data sets used in this report are of the order of two days. Thus, Figure 12 and 13 show that the harmonic analysis of these data should be reasonably accurate but that the time length of the data is short enough to be questionable. However, the data values used in these experimental data are not evenly spaced in time as is the case for the ficticious data. In order to better approximate the actual data, ficticious data values were selected at times which closely corresponded to the times of the actual data. Harmonic analyses were performed on these ficticious data and standard deviations were calculated as shown in Table 3. The smaller number of data points for each site corresponds to the basic time interval whereas the larger number of data points corresponds to the extended data.

In comparing the standard deviations in Table 3 of the basic and extended time intervals, one sees that the standard deviations may be reduced in some cases as much as 25% to 30%. The magnitude of these reductions are very significant.

An example of the comparison of an harmonic analysis of the experimental data for the two time intervals is shown in Figure 14. This figure shows the northward wind component from White Sands, set 1. The basic time length of the data was 2 days. Although the two data sets give similar results, there are definite differences. The amplitudes of the basic time interval are about 25% smaller at the higher heights and the phase is much more erratic than that of the extended time interval. These results indicate that one should definitely include the additional data scattered close in time around the basic time interval in the harmonic analyses of the atmospheric data. One must be careful, however, to keep the extended time interval short

43

TABLE 3. COMPARISON OF STANDARD DEVIATIONS OF BASIC AND EXTENDED DATA

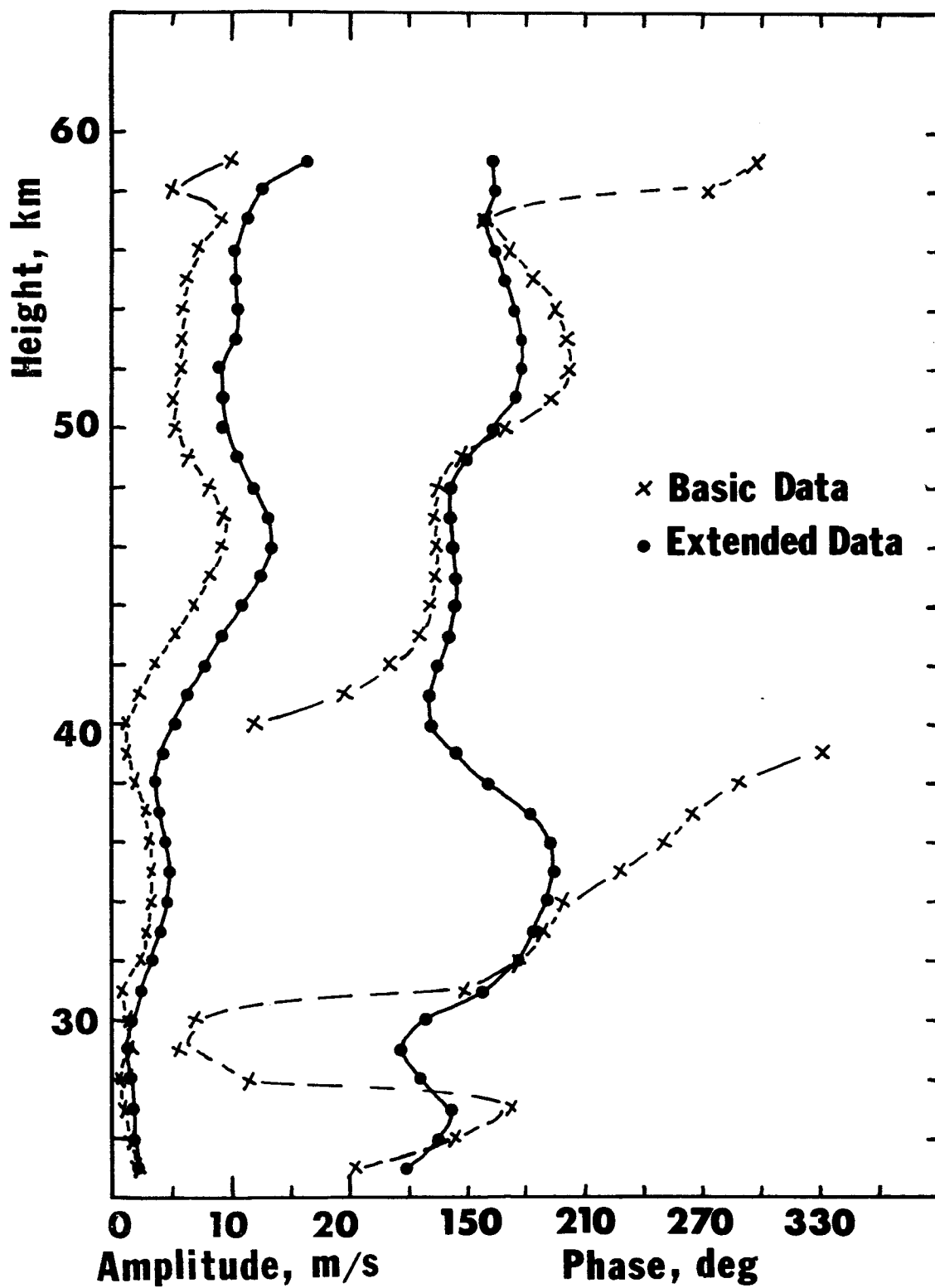| Number of Data Points	Diurnal Wind (m/sec)	Diurnal Wind Phase (Deg.)	Semidiurnal Wind (m/sec)	Semidiurnal Wind Phase (Deg.)
		Ascension Island		
24	1.38	10.92	2.55	57.67
32	1.33	10.19	2.47	47.07
		White Sands, Set 1		
20	2.51	13.26	2.12	30.64
35	2.03	10.33	1.92	22.39
		White Sands, Set 2		
17	2.12	18.76	2.62	45.27
28	1.55	12.01	2.08	37.11
		White Sands, Set 3		
13	2.73	18.03	2.29	36.01
25	2.48	15.45	1.98	24.92
		Fort Churchill		
19	1.93	13.76	2.16	48.66
22	1.99	12.49	2.15	32.75

Figure 14. Comparison of Harmonic Analysis of Basic and Extended Data for the Diurnal Northward Wind at White Sands, Data Set 1.

enough so that seasonal changes in tidal phase or amplitude would be small.

Time Structure Analysis. Harmonic analyses were performed on the five sets of data with the above mentioned corrections. The results were subtracted from the data which were corrected for solar radiation only; and thus, irregular data profiles were obtained. Then these irregular profiles were used in the time structure function to give an estimate of the gravity wave amplitudes as shown in Figure 1. The harmonic analysis results compared favorably with previous work that had been performed on essentially the same data[20-25].

Compatibility of Wind and Thermodynamic Data. A major difficulty in performing the harmonic analysis of upper atmospheric data is the insufficient quantity of properly space time series data. However, the need for the large quantity of data could possibly be reduced if the number of independent variables in the tidal equations of motion could be reduced.

In theory it is possible to infer temperature, pressure, and density data from the wind data[20,26]. In general, the process involves substitution of the wind component data into the east-west equation of motion to obtain geopotential height variations at several pressure levels. Then, these height variations are converted into pressure, density, and temperature variations. This method would make the pressure, density, and temperature variations dependent on the wind variations and thus, would certainly reduce the number of independent variables in an harmonic analysis. However, the method is very sensitive to errors in the wind components. To check the feasibility of applying this method to the data in the present report, we used the method to calculate the temperature, pressure and density variations from the observed wind variations for one data set from White Sands and then,

46

compared these results with the observed thermodynamic data. The comparison

of the two results was very poor. Similar results were obtained by Beyers et

al.[20]. Consequently, the conclusion of this analysis is that this method

should not be used as a means of reducing the number of independent variables

because it seems to be too sensitive to errors.

Another means to reduce the number of independent variables is to restrict

the phase difference between the northward and eastward wind components to

90°. Theory predicts that if the tidal motion contains only one mode of

oscillation, the zonal and meridional wind components will be in phase quad-

rature. However, if more than one mode of oscillation is present, the phase

relationship between the zonal and meridional wind could take on any value.

Inspection of the results of the tidal analysis from the five data sets in

the present report indicates that there is no consistent phase relationship

between the zonal and meridional wind components. Thus, this indicates that

more than one mode is present in the tidal motion and the phase difference

restriction to a value of 90° would be invalid.

Thus, the conclusion is that, at present, there is no means to by-pass

the need for the large quantity of properly spaced data in order to perform

the tidal harmonic analysis.

6. LONG PERIOD VARIATIONS

Sufficient MRN data were found for three sites to perform harmonic analysis using periods of 5 days and longer. The data were chosen for each site such that the data values occurred at the same time of day, plus or minus ten minutes, for a time interval covering about six years, 1964 through 1969. The sites and the local times of day were Ascension Island, A.F.B., 1345 hours; Cape Kennedy, Florida, 1000 hours; and Fort Greely, Alaska, 1000 hours. Site latitudes and longitudes are given in Table 1.

No solar radiation corrections were made on the temperature data since the corrections for solar angle variation at the same time of day throughout a year are quite small. The radiation errors would be essentially uniform in the data and would not affect the harmonic analysis. The only non-uniform radiation errors in the temperature data would be errors due to seasonal variations of the solar angle which are relatively small (less than $2^{o}K$ or about 0.8%).

The number of data points for the analysis vary with height from a maximum of 409 to a minimum of 65. The distribution of these data with seasons of the years are as follows:

	Winter	Spring	Summer	Fall
Ascension Island	26%	18%	30%	26%
Cape Kennedy	30%	22%	22%	26%
Fort Greely	24%	35%	25%	16%

The data are rather evenly distributed by seasons.

Harmonic analysis was performed by fitting one period at a time to the data and thus, a periodogram was obtained. The heights included in the analysis were 45 km through 60 km in increments of 5 km. For example Figures 15 through 23
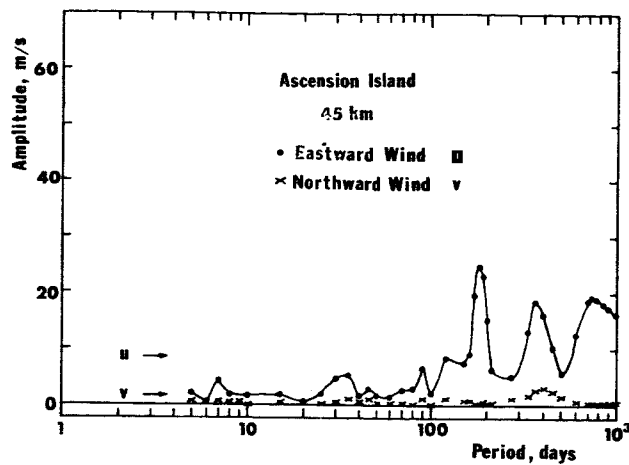
Figure 15. Periodogram of Wind Components for Ascension Island.
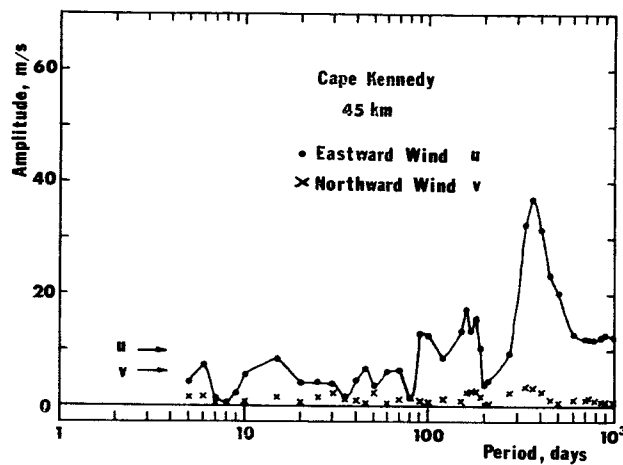
Figure 16. Periodogram of Wind Components for Cape Kennedy.
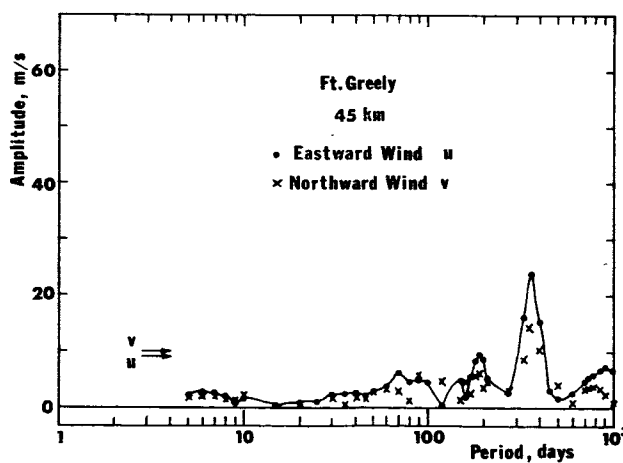
Figure 17. Periodogram of Wind Components for Fort Greely.

49

Figure 18.   Periodogram of Temperature for Ascension Island.

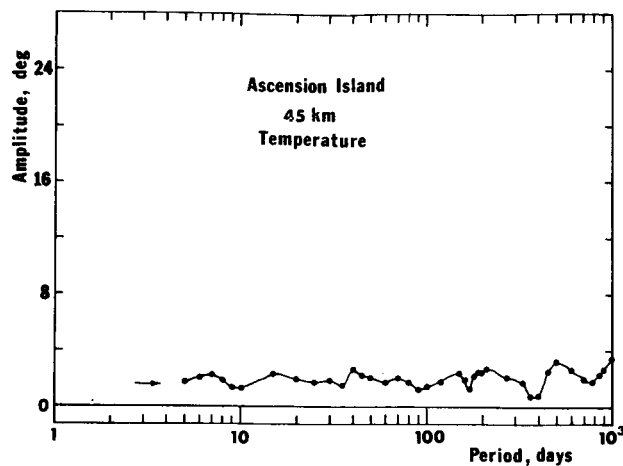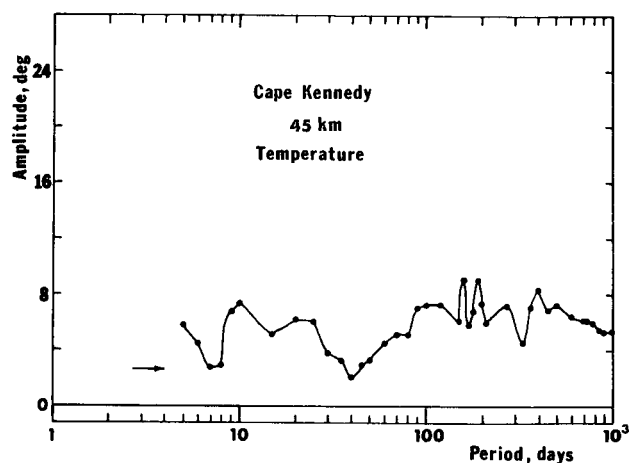Figure 19.   Periodogram of Temperature for Cape Kennedy.
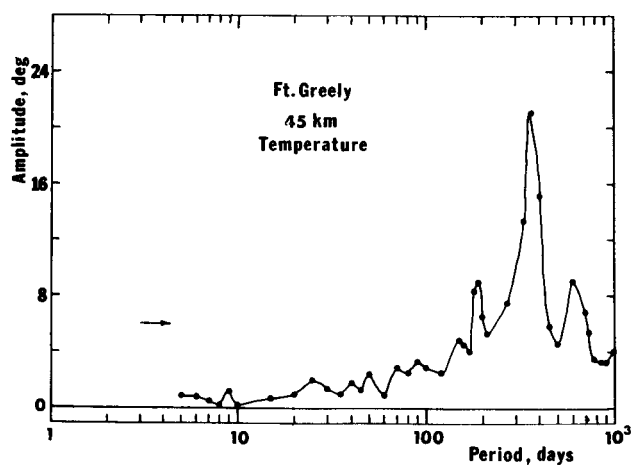
Figure 20.   Periodogram of Temperature for Fort Greely.
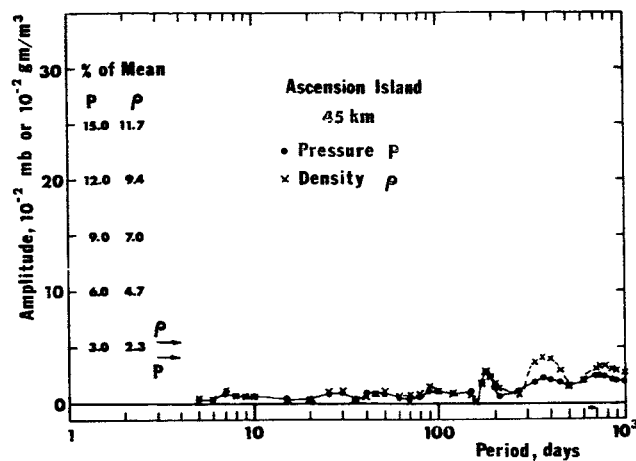
Figure 21. Periodogram of Pressure and Density for Ascension Island.
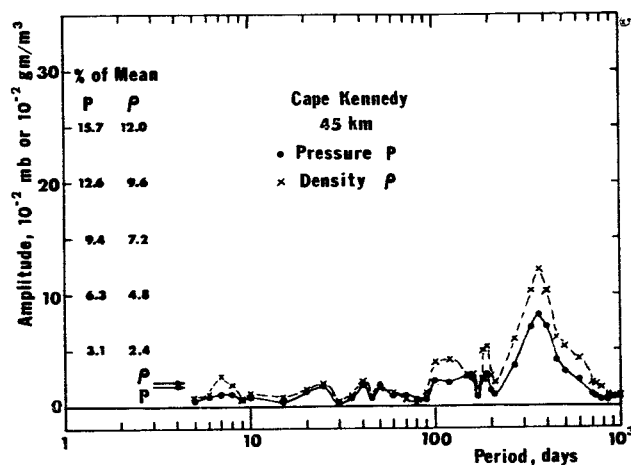
Figure 22. Periodogram of Pressure and Density for Cape Kennedy.
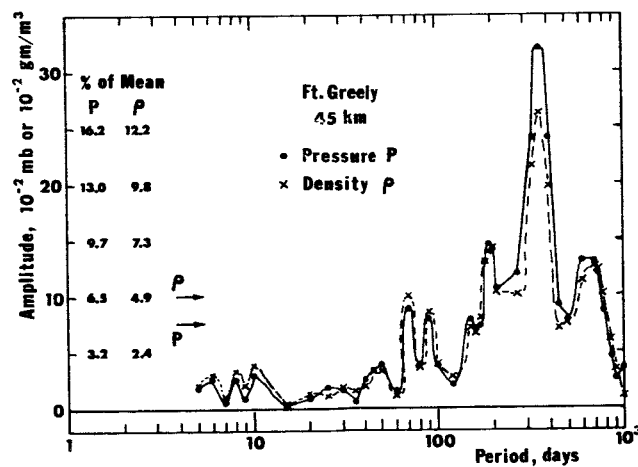
Figure 23. Periodogram of Pressure and Density for Fort Greely.

show the periodiograms for the winds, temperature, pressure and density at the height 45 km. The predominant oscillations shown by these figures are the annual, semi-annual, and quasi-biennial (period = 780 days) oscillations. The temperature seems to have a strong oscillation at the 600 days period also. Notice that the long period northward wind is very small compared to the eastward wind both at Ascension Island and Cape Kennedy and only becomes significant at the higher latitude of Fort Greely.

Quasi-biennial Oscillations. The quasi-biennial oscillation appears as definite peaks on the periodograms of the winds, pressure and density. The temperature curves do not show any preference for the quasi-biennial period as compared to adjacent periods. Table 4 shows the amplitude variations of this oscillation with height and latitude. Generally, the oscillation decreases in amplitude with increasing heights near the equator and increases im amplitude with increasing height at the higher latitudes. These results are in agreement with previous work[27-35]. Figure 24 shows the month of maximum amplitude of the quasi-biennial oscillation for the different sites. The abscissa of this figure has two scales. The top scale shows the month of maximum amplitude in the years 1966-1968 as calculated. The bottom scale shows the month of maximum amplitude for the years 1972-74 assuming that the oscillation remains coherent.

Annual Oscillation. The annual oscillation is definitely the most predominant of all the planetary waves as shown by the periodograms. Figure 25 shows the month of maximum amplitude for the different sites. Table 5 shows the variations of the amplitudes with height and latitude. The wind amplitudes for each site are rather constant with height. The eastward wind

52
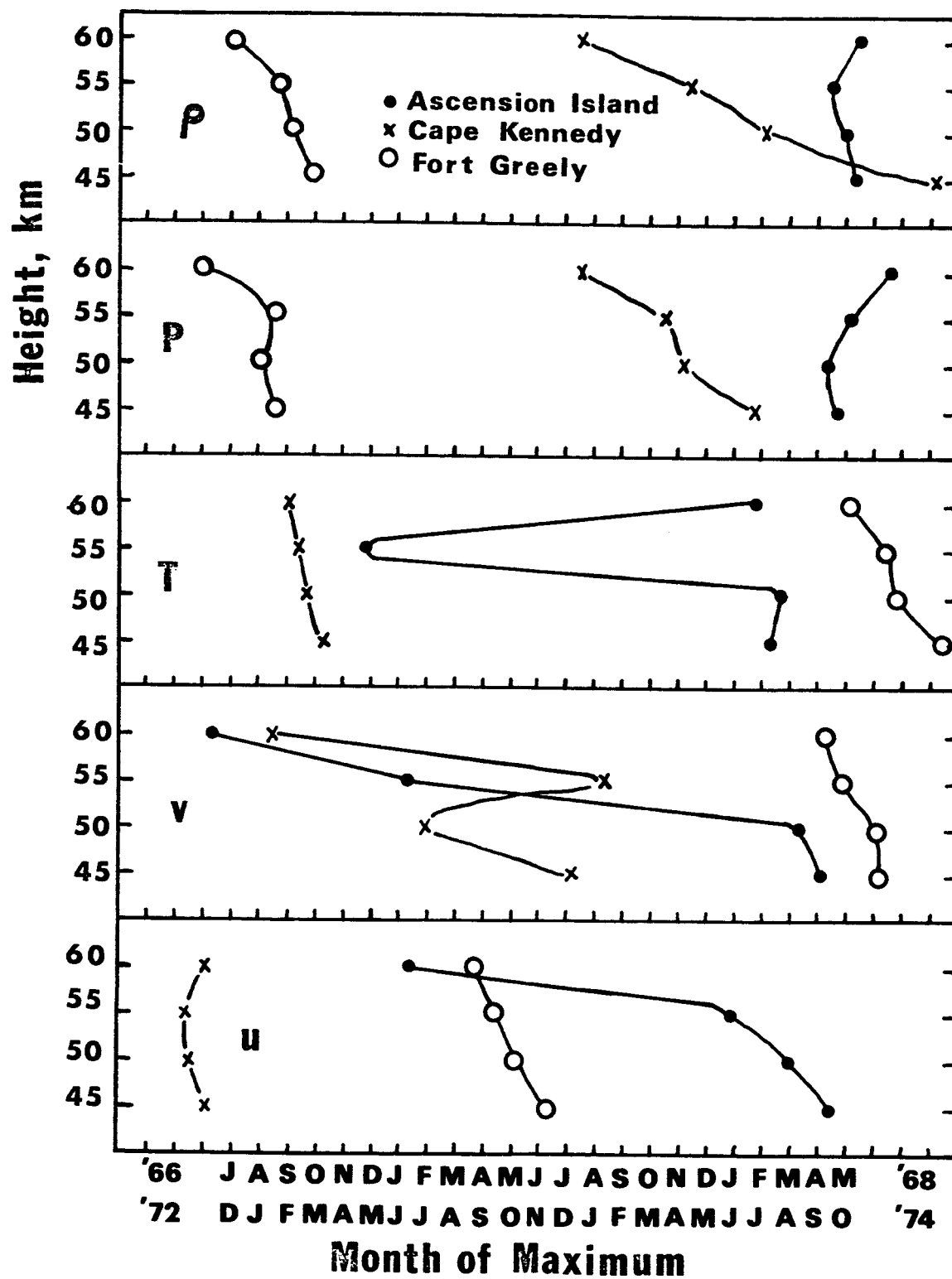
Figure 24. Month of Maximum for Quasi-Biennial Oscillations.
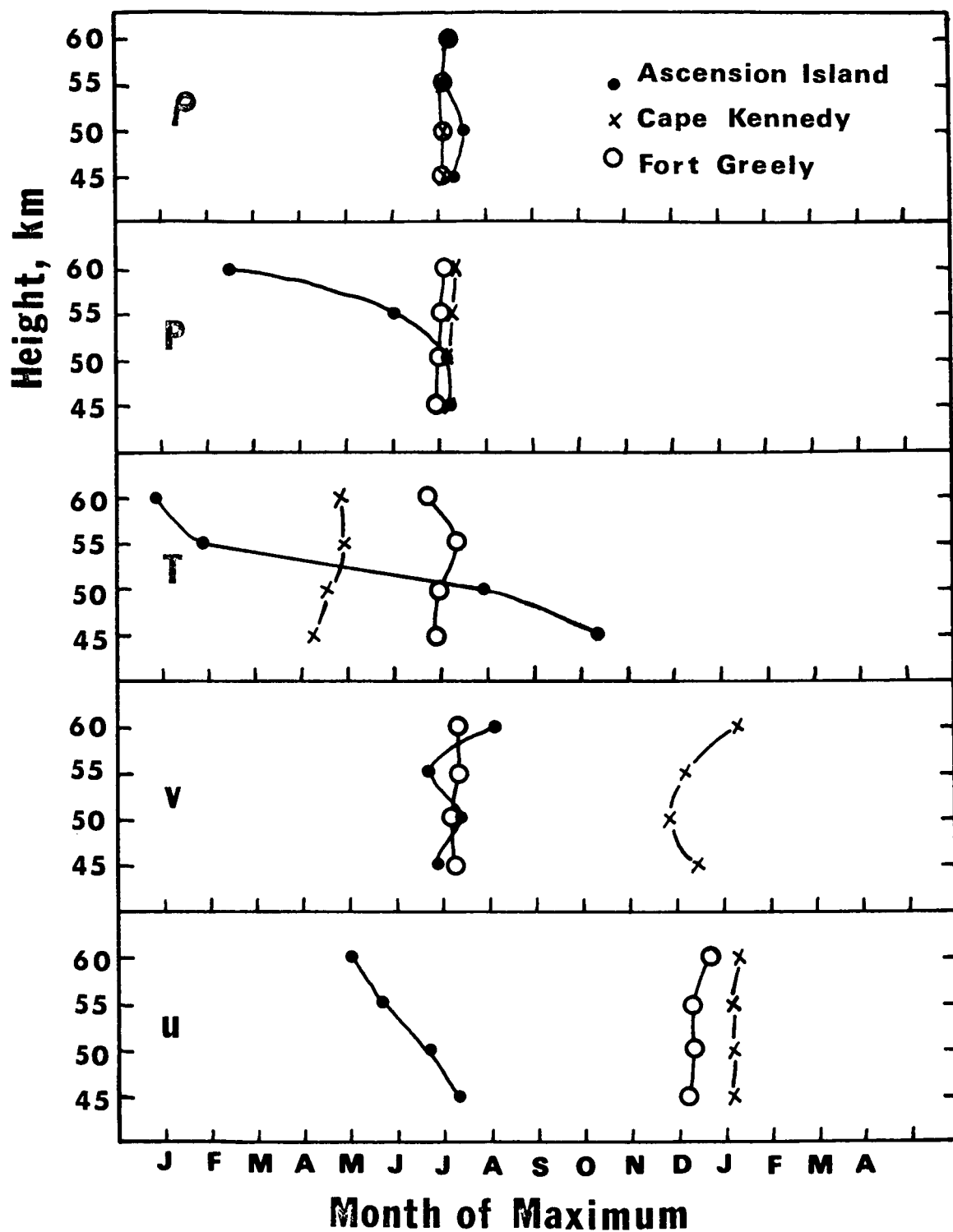
Figure 25. Month of Maximum for Annual Oscillations.

TABLE 4. AMPLITUDE VARIATION WITH HEIGHT
AND LATITUDE OF QUASI-BIENNIAL OSCILLATION

Height (km)	Ascension Island	Cape Kennedy	Fort Greely
Eastward Wind (m/sec)			
45	19.2	11.9	5.9
50	15.5	15.9	7.6
55	5.9	16.2	11.4
60	1.5	34.5	16.4
Northward Wind (m/sec)			
45	0.55	1.15	3.92
50	1.17	0.78	3.86
55	1.19	0.35	7.21
60	2.62	4.65	14.87
Temperature (K deg)			
45	1.86	5.97	3.56
50	1.87	4.46	4.08
55	0.64	8.03	4.13
60	0.84	17.89	6.45
Pressure (% of mean)			
45	1.5	0.3	5.6
50	1.4	0.8	7.0
55	1.2	1.2	7.6
60	0.9	1.9	8.4
Density (% of mean)			
45	1.5	0.8	5.0
50	1.5	0.5	6.5
55	1.3	0.9	7.5
60	1.8	1.5	6.5

TABLE 5.   AMPLITUDE VARIATION OF ANNUAL OSCILLATION WITH HEIGHT AND LATITUDE

Height (km)	Ascension Island	Cape Kennedy	Fort Greely
Eastward Wind (m/sec)			
45	18.4	37.0	23.8
50	16.6	42.6	26.8
55	17.8	43.0	29.0
60	14.4	40.1	22.3
Northward Wind (m/sec)			
45	2.9	3.2	13.9
50	2.9	2.8	15.8
55	3.1	2.2	15.1
60	3.0	2.3	14.6
Temperature (K deg)			
45	0.7	7.0	21.1
50	1.1	4.3	16.6
55	1.8	7.8	12.6
60	2.9	21.7	9.6
Pressure (% of mean)			
45	1.4	5.1	20.9
50	1.0	4.9	25.5
55	0.5	4.8	28.7
60	0.7	3.6	28.4
Density (% of mean)			
45	1.9	5.9	12.8
50	1.2	5.1	19.2
55	1.1	4.7	23.7
60	1.7	4.0	24.7

has its largest oscillations at Cape Kennedy. The northward wind is insignificant for the two lower latitude sites but becomes appreciable at Fort Greely.

The temperature oscillations, which are in units of K deg, and the pressure and density oscillation, which are in units of per cent of the mean, behave in similar fashions. Their amplitudes are small near the equator (less than 3) but increasing with latitude to an amplitude in the 20's at Fort Greely. These oscillations agree reasonably well with the results of Cole[34].

Semiannual Oscillation. The semiannual oscillations seem to be subordinate to the annual oscillations everywhere except near the equator. At the site of Ascension Island (especially in the eastward wind), the semiannual amplitudes are larger than the annual amplitudes at the lower heights. However, the semiannual amplitudes decrease rapidly with height so that the annual oscillations appear to dominate at the higher heights even near the equator.

Figure 26 shows the month of maximum amplitude for the different sites. Table 6 shows the amplitude variations with height and latitude. The eastward wind, as stated above, seems to decrease im amplitude with increasing height, but shows a maximum at the height of 50 km which agrees with experimental results of Reed[36]. The eastward wind amplitude remains essentially constant with height at Cape Kennedy and seems to increase with height at Fort Greely. The northward wind amplitude again is insignificant for the two lower latitudes but does become significant at Fort Greely.

Again, the temperature, pressure and density oscillations act similarly by having small amplitudes near the equator but increasing with latitudes to amplitudes of 10 to 15 at Fort Greely[34,35].
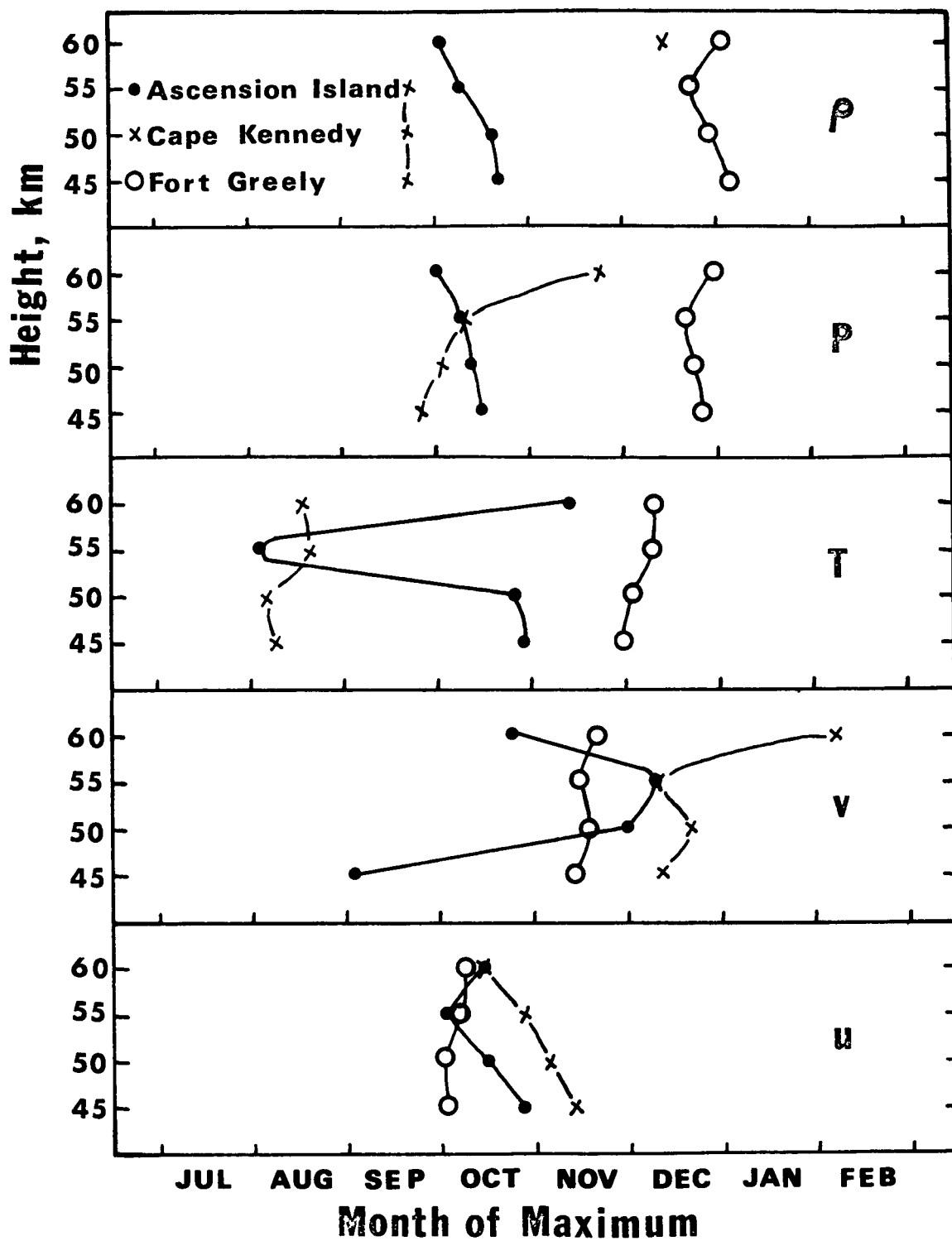
Figure 26. Month of Maximum for Semiannual Oscillations.

58

TABLE 6. AMPLITUDE VARIATION OF SEMIANNUAL OSCILLATION WITH HEIGHT AND LATITUDE

Height (km)	Ascension Island	Cape Kennedy	Fort Greely
Eastward Wind (m/sec)			
45	24.9	15.7	8.3
50	25.8	17.9	11.7
55	18.5	17.7	15.2
60	8.9	18.2	19.9
Northward Wind (m/sec)			
45	0.3	2.4	5.9
50	0.5	2.9	5.2
55	1.0	2.9	4.3
60	1.9	2.2	2.6
Temperature (K deg)			
45	2.2	6.8	8.3
50	1.8	3.8	7.9
55	1.4	7.0	7.2
60	2.7	22.8	4.8
Pressure (% of mean)			
45	1.7	1.5	8.4
50	1.8	1.4	10.5
55	1.4	1.3	13.7
60	1.1	0.7	15.8
Density (% of mean)			
45	1.3	2.4	6.3
50	1.5	1.8	8.0
55	1.8	1.0	10.9
60	1.0	0.8	14.3

<u>Shorter Period Oscillations.</u> Theories have been presented[37-40] which

predict that planetary waves of periods 5 to 50 days may penetrate upward into

the stratospheric regions. A few observations have been made which seem to

substantiate these theories[41, 42] and recent refinements to the theory have

been offered[43]. In the present analysis, attempts to identify planetary waves

of periods 5 to 50 days from the periodograms were made. There seem to be indi-

cations in the periodograms of oscillations with these periods; however, the

oscillations are not consistent for the different sites or for the different

parameters. For example, oscillations with periods of about 6 days and 25 days

appear to peak in the eastward wind at Cape Kennedy with an amplitude of about

10 m/sec, but not at the other two sites. In addition, the other parameters

do not show peaks at these two periods except possibly the pressure and density

oscillations at Fort Greeley.

The periodograms indicate that the largest oscillations in the wind and

temperature in the periodic range of 5 to 50 days occur at Cape Kennedy with

amplitudes of about 10 m/sec and 7 K deg. The other two sites show very small

oscillations in the winds and temperatures for these periods. The oscillations

in pressure and density seem to be largest at Fort Greely with amplitudes of

about two per cent of the mean and seem to be smallest at Cape Kennedy.

The amplitudes of the 14 to 30 day periods were analysed also by the meth-

od of daily differencing (See Section 3). These amplitudes are shown for com-

parison in Figures 15 through 23 by the arrows on the left side of the figures.

In every case except two, the amplitudes as shown by the periodograms are

much smaller than those predicted by the daily difference method. The prob-

able cause for the discrepancy is that the harmonic analysis method assumes

that the oscillations remain coherent for the entire time of investi-

gation. It is highly unlikely that a planetary wave of period 5 to 50 days would remain coherent for six years. Thus, if the waves were incoherent, the harmonic analysis method would underestimate the amplitudes of these waves. To do a harmonic analysis for these planetary waves, one needs to divide the data into smaller time intervals so that coherence could be attained. Then, the results of all the time intervals could be averaged.

7. SOLAR CORRELATIONS

Correlation at Chemical Release Heights. A significant correlation has been found[44] between the northward wind component and the $F_{10.7}$ solar flux (or Zurich sunspot number R_z) in the altitude range 110 - 140 km. Density and temperature variations near the 100 km level have also been correlated with solar activity[45]. The eastward wind component, however, was not found to be correlated with solar activity indices in a significant way. The northward wind correlation was such as to give a regression relation

$$V_N = 42 + 0.85 \ F_{10.7} \tag{35}$$

Since the average value of $F_{10.7}$ is approximately 80, a 10% change in $F_{10.7}$ would cause a change of roughly 7% in the northward wind component.

It is believed that the dependence of northward velocity on $F_{10.7}$ expressed by equation (35) is the result of the generation of gravity waves by magnetic storms and their subsequent propagation equatorward. The southward propagating gravity waves would produce a predominately north-south velocity perturbation. The generation of gravity waves by magnetic substorms was proposed earlier by Testud and Vasseur[46].

Observations of increased eastward wind components at higher altitudes (near 160 km) during a geomagnetic storm were reported by Smith[47] but the increased eastward component was suggested as being due to a thermal wind relationship with increased polar temperature over equatorial temperature.

A solar cycle dependence of prevailing winds (both northward and eastward components) and semidiurnal component winds have been reported by Springer and

Schminder[48]. These observations at about 95 km altitude indicate an increase in the semidiurnal component with solar activity, but a decrease of the prevailing winds with solar activity.

It was decided that, rather than a correlation analysis, a superposed epoch analysis, similar to that applied by Woodbridge[49] at the 300 mb level, would be most appropriate. The superposed epoch analysis would consist of mean square values of a parameter (e.g. gravity wave or planetary wave wind or thermodynamic variables) plotted versus number of days before or after a key day, i.e. a day of high solar activity. However, it was considered that at this time the amount of data above MRN height, is such that too few data would be from times close to key days for such an analysis to be performed (See below for discussion of the method of key day selection). Thus the superposed epoch analysis above 65 km was postponed until more data can be added to that already accumulated. In the meantime it is felt that the correlation given by equation (35) can be used to estimate the gravity wave magnitude through

$$\Delta V_N = 0.85 \ \Delta F_{10.7}.$$

Correlation at MRN Heights. The superposed epoch analysis was employed on the MRN data from three sites: Ascension Island, Cape Kennedy, and Fort Greely. The first problem was to define the key days to be used in the analysis. Noonkester[50] used as a definition any day in which the international character figure C_i increased by 1.0 or more from the preceding day. Woodbridge[49] considered as a key day any day on which the planetary geomagnetic index A_p was 15 or larger and had first reached this value through a one-day rise ΔA_p greater than 11. The Noonkester definition yielded 56 key days in the 1964-69 period studied, or about one every 39 days on the average. The Woodbridge de-

finition yielded 151 key days or about one every 14 or 15 days on the average. Therefore a modified definition was developed to reconcile these differences. The following definition was adopted: A key day is one in which A_p is greater than 15 and first became greater than 15 through either (1) a one-day change $\Delta A_p \geq 11$ and on which also the one-day change $\Delta C_i \geq 1$, or (2) a one day change $\Delta A_p \geq 18$ regardless of the ΔC_i value. With this definition 50 of the 56 $\Delta C_i \geq 1$ days corresponded to $\Delta A_p \geq 11$ days and there were 28 additional $\Delta A_p \geq 18$ days which did not correspond to $\Delta C_i \geq 1$, with a total of 78 key days. Table 7 gives a yearly and monthly breakdown of the occurrence of key days determined by this method.

After the key days had been selected, daily difference magnitudes in the 25 to 45 km and 45 to 65 km height ranges were averaged with respect to number of days before or after a key day (based on the date of the earlier profile of the pair being differenced). Daily differences over one day separation, to check for gravity wave dependence on solar activity, and over 7 to 15 days separation, to check for planetary wave dependence on solar activity, were tested. In all cases, in both height ranges, no significant variation of magnitude with respect to days after a key day was determined.

Thus it appears, on the basis of this study, that the solar correlation found near the 100 km level[44,45] and that found at lower stratospheric heights[49-52] are not connected by processes which propagate through the 25 – 65 km region. This supports the idea that the correlations near the 100 km level are due to direct geomagnetic storm generation of gravity waves[46], while the lower stratospheric, and possibly surface correlations are due to a complicated chain of x-ray nucleation, cloud formation, and surface radiation balance effects, such as proposed by Roberts[51].

64

TABLE 7. YEARLY AND MONTHLY DISTRIBUTIONS
OF THE 78 KEY DAYS

Year	Number	Month	Number	Month	Number
1964	17	Jan.	6	July	6
1965	7	Feb.	12	Aug.	5
1966	15	Mar.	9	Sept.	9
1967	16	Apr.	6	Oct.	6
1968	11	May	9	Nov.	2
1969	12	June	4	Dec.	4

It will be possible, with the addition of a few more data sets, to do a superposed epoch analysis of winds in the chemical release altitude region. With this approach it should be possible to compute gravity wave magnitudes during geomagnetic storms and during non-storm conditions.

8. PROCEDURE FOR EVALATION OF EFFECTS ON SPACECRAFT DUE TO ATMOSPHERIC VARIATION

The analysis of structure functions indicate that the gravity wave perturbations in wind, pressure, density, and temperature in the 25 - 200 km region have a continuous spectrum. Thus the effects of gravity waves on a spacecraft traversing these altitudes can be analyzed in terms of the spectral techniques of turbulence.

Planetary waves in the 45 - 65 km region exhibit single modes of specific vertical wavelength (above 37 km) and in the 65 - 85 km region a preferred vertical wavelength of about 20 km is found for the planetary scale waves. Atmospheric tides also exhibit discrete wavelengths. Statistical but non-spectral methods for considering these discrete wavelength phenomena are presented later in this section.

The coordinates of the analysis are indicated in Figure 27. The x, y, z system has x and y axes in the horizontal plane and z in the vertical direction. The x direction has been conveniently chosen to be along the azimuth of the spacecraft trajectory. The elevation of the spacecraft trajectory is the angle θ and the x', y', z' axes are those which are rotated through this angle θ. Thus x' is along the direction of flight of the spacecraft. The displacement r along the x' axis is the distance of travel of the spacecraft in an arbitrary time interval τ. With the speed of the spacecraft given by U, then r and τ are related by $r = U\tau$. The displacement r can be broken into component displacements r_1 and r_3 in the horizontal and vertical directions given by

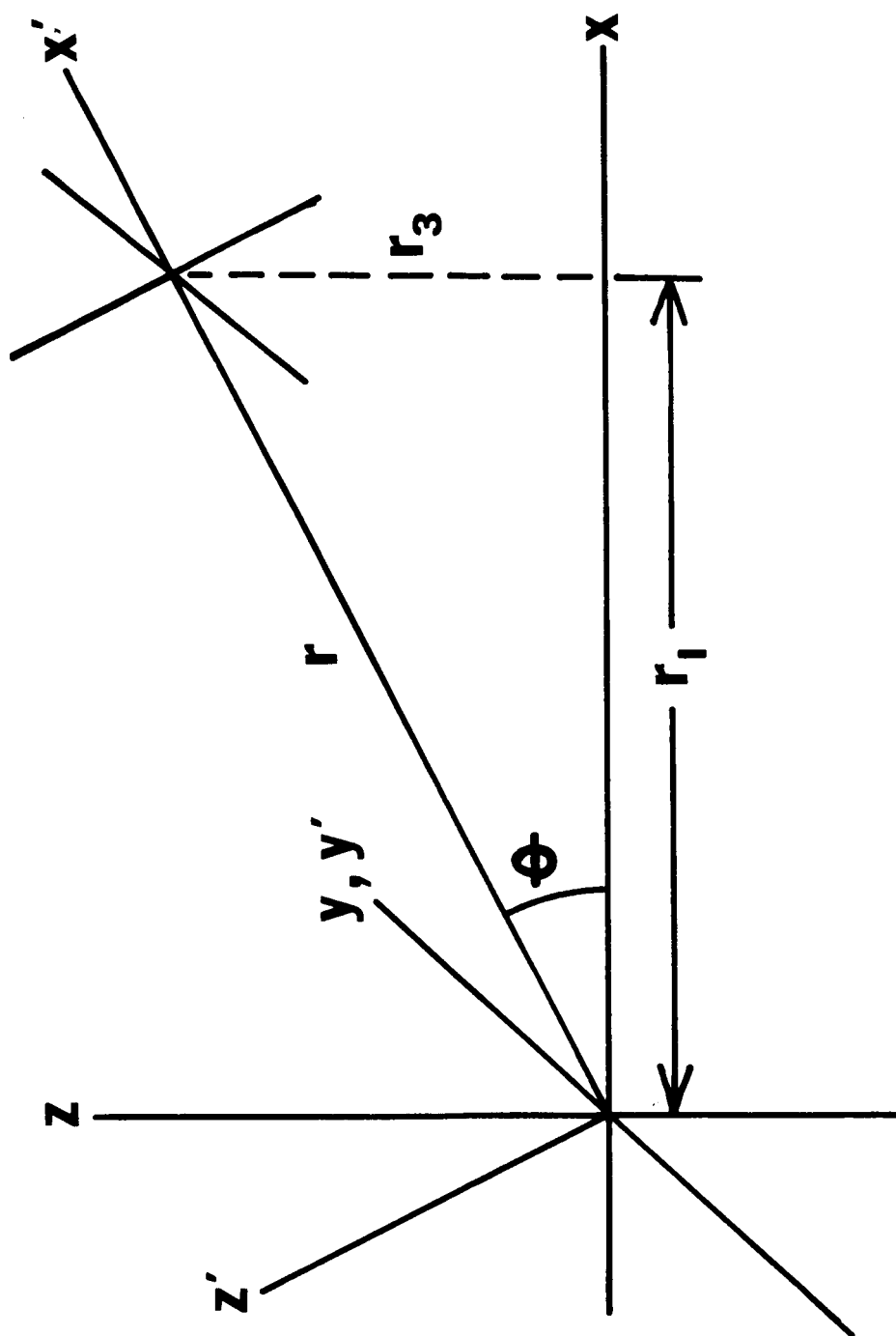$$r_1 = U \cos \theta \, \tau \qquad r_3 = U \sin \theta \, \tau \qquad (36)$$

Figure 27. Coordinate systems used in the analysis of effects on spacecraft due to atmospheric variation. Elevation of trajectory is angle θ, displacement r is along trajectory path.

<u>Correlation Functions</u>. The structure functions measured and reported both in section 3 and 4 and in the earlier report[1] can be related to correlation functions, which in turn can be related to spectra. The measurements indicate that both scalar and vector spectra should have a high frequency range power law behavior with exponents ranging from -1.6 to -2.5. The high frequency range exponent for the von Karman spectrum is -1.67 and for the Dryden spectrum it is -2.0. The Dryden spectrum, which is based on a linear exponential correlation function, is often used in place of the von Karman spectrum for atmospheric turbulence and the differences between the two have little engineering significance because the major differences occur only at the relatively unimportant high frequencies. Since the Dryden exponent falls roughly in the middle of the observed range of exponents then the Dryden spectrum can be used in all cases without serious engineering error. However, the anisotropy of the irregular variation fields must be taken into account by the use of different vertical and horizontal scales.

For engineering purposes the following spatial correlation functions can be used in the 25 to 200 km altitude range: For scalar quantities (pressure, density, and temperature) use

$$R(\underset{\sim}{r}) \;=\; e^{-r/L} \tag{37}$$

where r/L is given by

$$(r/L)^2 \;=\; (r_1/L_1)^2 + (r_3/L_3)^2 \tag{38}$$

and L_1 and L_3 are respectively the horizontal and vertical scales given in Table 8 for gravity wave pressure, density, and temperature variations. Substitution of (36) into (38) provides a relation between the length scales

69

and the trajectory angle θ

$$L = L_1 L_3 / (L_1^2 \sin^2 \theta + L_3^2 \cos^2 \theta)^{1/2} \tag{39}$$

For spatial correlations of velocity components use

$$R_{11}(\underset{\sim}{r}) = (1 - r_3^2 / 2rL_u) e^{-r/L_u} \tag{40}$$

$$R_{22}(\underset{\sim}{r}) = (1 - r/2L_u) e^{-r/L_u} \tag{41}$$

$$R_{33}(\underset{\sim}{r}) = (1 - r_1^2 / 2rL_w) e^{-r/L_w} \tag{42}$$

$$R_{13}(\underset{\sim}{r}) + R_{31}(r) = (r_1 r_3 / rL_w) e^{-r/L_w} \tag{43}$$

where $R_{ij}(\underset{\sim}{r})$ is the correlation $\langle u_i(\underset{\sim}{x}) u_j(\underset{\sim}{x} + \underset{\sim}{r}) \rangle / \sigma_i \sigma_j$, σ_i is the rms value of the ith velocity component, and L_u and L_w are defined by

$$(r/L_u)^2 = (r_1/L_{u1})^2 + (r_3/L_{u3})^2 \tag{44}$$

$$L_u = L_{u1} L_{u3} / (L_{u1}^2 \sin^2 \theta + L_{u3}^2 \cos^2 \theta)^{1/2} \tag{45}$$

$$(r/L_w)^2 = (r_1/L_{w1})^2 + (r_3/L_{w3})^2 \tag{46}$$

$$L_w = L_{w1} L_{w3} / (L_{w1}^2 \sin^2 \theta + L_{w3}^2 \cos^2 \theta)^{1/2} \tag{47}$$

where L_{u1}, L_{u3}, L_{w1}, and L_{w3} are horizontal and vertical scales given in Table 8, along with the appropriate mean σ values for the irregular horizontal winds u and v (u_1 and u_2) and vertical component w (u_3).

Scalar and Velocity Spectra. Spectra computed from these correlation functions are as follows: For the spectrum of scalar quantities use

70

$$\phi(k) = 2\sigma^2 L/\pi[1 + (kL)^2] \tag{48}$$

where σ is the rms value of the quantity whose spectrum is being evaluated. The wave number spectra in (48) is for k in radians/km, with L determined from (39), or in terms of frequency ω in radians/sec use

$$\phi(\omega) = 2\sigma^2 L/\pi U[1 + (\omega L/U)^2] \tag{49}$$

Table 8 gives values of σ for gravity wave pressure, density and temperature variations. For trajectory angles θ less than about 5° the spectrum computed by either (48) or (49) can be considered the same as for level flight, i.e. use L_1 for L. The trajectory angle θ is less than 5° throughout the entire descent phase and above 85 km on the ascent phase of the typical space shuttle trajectory (see Table 9 for the typical values used here). For the transverse velocity spectrum in the horizontal direction use

$$\phi_{22}'(k) = \sigma_u^2 L_u[1 + 3(k L_u)^2]/\pi[1 + (k L_u)^2]^2 \tag{50}$$

for the wave number spectrum with L_u determined from (45) or in terms of frequency use

$$\phi_{22}'(\omega) = \sigma_u^2 L_u[1 + 3(\omega L_u/U)^2]/\pi U[1 + (\omega L_u/U)^2]^2 \tag{51}$$

For trajectory angles less than 2° horizontal flight may be assumed and L_{u1} used for L_u in (50 or (51). For the transverse velocity spectrum in the vertical plane use

$$\phi_{33}{}'(k) = \frac{\sigma_w{}^2 \cos^2 \theta \; L_w[1 + \sin^2 \theta + (2 + \cos^2 \theta)(k \; L_w)^2]}{\pi \; [1 + (k \; L_w)^2]^2}$$

$$+ \frac{\sigma_u{}^2 \sin^2 \theta \; L_u[1 + \cos^2 \theta + (2 + \sin^2 \theta)(k \; L_u)^2]}{\pi \; [1 + (k \; L_u)^2]}$$

$$- \frac{2\sigma_u \sigma_w \sin^2 \theta \cos^2 \theta \; L_w[1 - (k \; L_w)^2]}{\pi \; [1 + (k \; L_w)^2]} \tag{52}$$

For $\theta < 2^{\circ}$ horizontal flight may be assumed and (52) reduces to

$$\phi_{33}{}'(k) = \sigma_w{}^2 \; L_{w1}[1 + 3(k \; L_{w1})^2]/\pi[1 + (k \; L_{w1})^2]^2 \tag{53}$$

or, expressed as a frequency spectrum

$$\phi_{33}{}'(\omega) = \sigma_w{}^2 \; L_{w1}[1 + 3(\omega \; L_{w1}/U)^2]/\pi U[1 + (\omega \; L_{w1}/U)^2]^2 \tag{54}$$

Because of small values of σ_w and L_w the transverse vertical spectrum computed by (52) remains a factor of ten or more smaller than the horizontal transverse spectrum $\phi_{22}{}'$ even up to trajectory angles of 15°. Therefore, the simple forms (53) or (54) may be used in all cases in which the vertical spectrum, because of its smaller magnitude, would not have to be evaluated with extreme accuracy.

The longitudinal spectrum would have a complicated angular form analogous to (52) but since it is no more angular sensitive that the transverse spectra, and since the longitudinal response modes are usually unimportant, only the level flight spectral form need be considered. With $\theta = 0$, the longitudinal spectrum is

$$\phi_{11}{}'(k) = 2\sigma_u{}^2 \; L_{u1}/\pi[1 + (k \; L_{u1})^2] \tag{55}$$

72

Table 8. Horizontal and vertical scales and mean standard deviation values for irregular winds, pressure, density, and temperature. Values in parentheses indicate interpolations, extrapolations, or values assumed by analogy with other variables.

Altitude Range	u and v			w			p			ρ			T		
	L_{u1}	L_{u3}	$\bar{\sigma}$	L_{w1}	L_{w3}	$\bar{\sigma}$	L_1	L_3	$\bar{\sigma}$	L_1	L_3	$\bar{\sigma}$	L_1	L_3	$\bar{\sigma}$
(km)	(km)	(km)	(m/s)	(km)	(km)	(m/s)	(km)	(km)	(%)	(km)	(km)	(%)	(km)	(km)	(%)
25 – 45	50	3	4	(10)	(3)	(1)	(50)	20	2	(50)	20	2	(50)	5	1.2
45 – 65	50	6	6	(10)	(6)	(2)	(50)	20	2	(50)	20	2	(50)	5	0.7
65 – 85	(100)	10	18	(15)	(10)	(5)	(100)	20	7	(100)	20	8	(100)	5	4
85 – 110	150	10	40	20	10	11	(150)	(20)	7	(150)	(20)	12	(150)	(5)	8
above 110	200	20	45	30	30	13	(200)	(40)	(15)	(200)	(40)	10	(200)	(10)	15

73

or in frequency form

$$\phi_{11}'(\omega) = 2\sigma_u^2 L_{u1}/\pi U[1 + (\omega L_{u1}/U)^2] \qquad (56)$$

TABLE 9. TYPICAL SPEEDS U AND TRAJECTORY ANGLES θ FOR SPACE SHUTTLE TRAJECTORIES.
Values were determined from Smith et al[53].

Height Range (km)	Ascent		Descent	
	U (km/sec)	θ (deg.)	U (km/sec)	θ (deg.)
45 – 65	2.4	14°	4.6	0.6°
65 – 85	3.4	7°	4.7	0.2°
85 – 110	5.9	2°	4.6	0.8°

Probabilities and Exceedance Values. No measurements have been made of the probability distribution of the standard deviation p(σ). Only the average values have been determined. The form of p(σ) which should be assumed is the same as used for turbulence at lower altitudes.

$$p(\sigma) = (\sqrt{2/\pi} \, b) \exp (-\sigma^2/2b^2) \qquad (57)$$

from which it can be shown that the average value of σ is $\bar{\sigma} = b\sqrt{2/\pi}$, so that the values of b (the standard deviation of σ) to be used are given by

$$b = \bar{\sigma}\sqrt{\pi/2} = 1.253 \, \bar{\sigma} \qquad (58)$$

where $\bar{\sigma}$ values can be obtained from Table 8. Therefore the number M of fluctuations of a load quantity y that exceed the value y* is given by

$$M(y^*) = N_o \exp(-|y^*|/1.253 \bar{\sigma} A) \tag{59}$$

where N_o is given by

$$N_o = (1/2\pi \sigma_y) \left[\int_0^\infty \omega^2 \phi_y(\omega) \, d\omega \right]^{1/2} \tag{60}$$

in which ϕ_y is the spectrum of y and σ_y is given by

$$\sigma_y = \left[\int_0^\infty \phi_y(\omega) \, d\omega \right]^{1/2} \tag{61}$$

For a single element of the spacecraft the relation between the spectrum $\phi_y(\omega)$ of the response y and the spectrum $\phi(\omega)$ causing the response is

$$\phi_y(\omega) = \phi(\omega) |H^2(\omega)| \tag{62}$$

where H is the transfer (frequency response) function. The parameter A in equation (59) is given by

$$A = \sigma_y/\sigma \tag{63}$$

Thus a standard type of exceedance model such as that employed by NASA[54] can be used with b, the standard deviation of σ, given by equation (53). With further study perhaps $p(\sigma)$ could be divided into quiet or non-storm conditions and active or storm conditions based on mid-winter warming conditions, especially at the lower altitudes, and based on solar activity, especially at the higher levels. Perhaps a better relation than (57) could be determined by actual measurement of the probability of occurrence of σ values. Seasonal variation of $p(\sigma)$ may also exist.

Latitude and Other Variations. If it is desired to take into account the different irregular variation magnitudes at various latitudes then the average standard deviation values from Figure 8 may be used in the 25 - 65 km altitude range.

75

If account is to be taken of the relative amount of time spent in the various flight regimes (latitude, altitude, etc.) then consider the case of a total of k mission segments, with time t_i spend in each mission segment, and a total flight time of T. The total exceedance rate for all mission segments is

$$M(y^*) = \sum_{i=1}^{k} (t_i N_{o_i}/T) \exp(-|y^*|/1.253 \, \bar{\sigma}_i A_i) \qquad (64)$$

and the parameters N_{o_i}, A_i, and $\bar{\sigma}_i$ are evaluated separately for each mission segment.

Dicrete Wave Phenomena. Although planetary scale waves and tides have horizontal wave lengths much larger than the gravity wave components, their vertical wavelengths may be comparable. For horizontal flight the presence of these other variations would not be important. However, in those cases in which the trajectory angle θ is small but non-zero the effects of the presence of these vertical variations can be important. It is suggested that, rather than use a discrete wavelength in a spectral approach, it would be more practical to consider only what mean square variation along the trajectory will occur. Consider a simple model in which some phenomenon f (e.g. a wind or thermodynamic variation due to tides or planetary scale waves) has a height and horizontal variation at a specific time given by

$$f(x, z) = A \sin(2\pi x/L_1) \sin(2\pi z/L_3) \qquad (65)$$

where x is along the trajectory direction, L_1 and L_3 are the horizontal (along x) and vertical wavelengths respectively, A is the amplitude, and the phase was selected arbitrarily. The mean square differences in the parameter f in going

76

from x to x + r_1 and z to z + r_3 can be determined by

$$\langle \Delta f^2(r_1, r_3) \rangle = \frac{1}{L_1 L_3} \int_0^{L_3} \int_0^{L_1} [f(x + r_1, z + r_3)$$

$$- f(x, z)]^2 \, dx \, dz \tag{66}$$

If equation (65) is substituted into (66) the result is

$$\langle \Delta f^2(r_1, r_3) \rangle = (A^2/2) [1 - \cos(2\pi r_1/L_1) \cos(2\pi r_3/L_3)] \tag{67}$$

In order to estimate mean square variations in winds, pressure, density and temperature due to tides and planetary scale waves in the 45 - 65 km region the magnitude values listed in Table 10 may be taken as representative. The planetary wave magnitudes shown in Table 10 are from Figure 2 and the tidal magnitudes are from the analysis results of Section 5. The most appropriate vertical wavelengths L_3, in the 45 - 65 km height range are: approximately infinite for the semidiurnal tide and the mid-and high latitude diurnal tide, and about 30 km for the low latitude diurnal tide. For the planetary scale waves in the 45 - 65 km height range $L_3 \simeq 37$ km may be used. Horizontal wavelengths for both the tides and planetary waves would be a few thousand kilometers, depending on the trajectory angle and the latitude.

The time structure function data shown in Figure 1 indicates fairly large magnitude gravity waves with a discrete period of 3 hours. The effects of this gravity wave mode may be accounted for by the same method just described except that the time variation must also be taken into account, since appreciable variation of this gravity wave component could occur during the time span of re-entry. Equation (67) may be generalized to accout for a time

TABLE 10. MAGNITUDES OF TIDAL AND PLANETARY WAVE
VARIATION IN THE 45 - 65 KM HEIGHT REGION

	Semidiurnal Tide			Diurnal Tide			Planetary Scale Waves		
	Low Lat.	Mid. Lat.	High Lat.	Low Lat.	Mid Lat.	High Lat.	Low Lat.	Mid. Lat.	High Lat.
A_u, m/s	1.1	3.6	2.3	2.5	7.4	4.2	10.0	9.7	8.1
A_v, m/s	1.5	2.6	2.1	2.9	9.0	5.8	1.1	6.3	9.8
A_p, %	0.3	3.7	1.6	2.9	5.1	2.5	0.4	3.6	6.3
A_ρ, %	0.4	3.9	1.7	2.4	4.2	1.0	0.6	2.7	6.9
A_T, %	1.5	3.1	1.2	3.1	5.9	3.2	0.4	0.9	1.7

difference τ by the relation

$$\langle \Delta f^2(r_1, r_3, \tau) \rangle =$$

$$(A^2/2) \, [1 - \cos(2\pi r_1/L_1) \, \cos(2\pi r_3/L_3) \, \cos(2\pi\tau/P)] \tag{68}$$

where the period $P = 3$ hours in this case. The amplitudes of the 3 hour grav-

ity wave components in the 45 – 65 km height range are estimated from Figure 1

to be $A_p = 4.2\%$, $A_\rho = 4.7\%$, $A_T = 3.2\%$, $A_u = A_v = 5.7$ m/s. The horizontal scale

L_1 is estimated to be $L_1 \simeq (A_u^2 + A_v^2)^{1/2} P \simeq 90$ km and the vertical scale L_3

is probably in the range of 5 to 10 km.

A Re-entry Trajectory Model. Consider a model similar to that of Campbell[55],

which divides the trajectory $x - z$ plane into discrete coordinate points x_i, z_j

where $x_i = x_o + i \, \Delta x$ and $z_j = z_o + j\Delta z$. We consider that a parameter, say den-

sity, evaluated at these points would be given by

$$\rho_{ij} = \bar{\rho}_{ij} + \rho'_{ij} + \Gamma_{ij} \tag{69}$$

where $\bar{\rho}_{ij}$ is the mean density appropriate to the height, latitude, and month or

season as determined by some reference or standard atmosphere. The component

ρ'_{ij} is a discrete wave component and may be evaluated by

$$\rho'_{ij} = \rho'_{oo} + A_\rho \{[1 - \cos(2\pi i\Delta x/L_1) \, \cos(2\pi j\Delta z/L_3)]/2\}^{1/2} \tag{70}$$

as from equation (67), or (68) for the 3 hour gravity wave component. Γ_{ij} repre-

sents the continuous spectrum gravity wave component and might be determined as

a set of random numbers selected from a gaussian distribution with the standard

deviation determined from Table 8. However, the Γ_{ij} values at neighboring points

must be correlated. The set of Γ_{ij} values can be made to have explicit corretion by

generating Γ_{ij} values from surrounding, previously generated values by the relation

$$\Gamma_{i+1, j+1} = \alpha \, \Gamma_{i, j+1} + \beta \, \Gamma_{i+1, j} + \gamma \, \epsilon \qquad (71)$$

where ϵ is an uncorrelated gaussian random variable with standard deviation given by Table 8 and α, β, and γ are determined from the known correlation between the adjacent points (given by equation (37) for scalar quantities or equation (40), (41), or (42) for velocity components) by methods developed by Hicks and Justus[56]. The spacecraft is then "flown" through an ensemble of sets of such density fields and the variation of trajectory parameters can be computed.

APPENDIX A.

ERROR ESTIMATE IN STANDARD DEVIATION
FROM MEASURED FOURTH MOMENTS

Consider a set of values X_i, $i = 1$ to n which have mean zero ($\bar{x} = \langle x \rangle = 0$) and variance σ^2 ($\langle x^2 \rangle = \sigma^2$). We now wish to compute an estimate of the error ε_σ in the measued value of σ. The variance of the set of data values is $v = \langle x^2 \rangle$ and the individual contributions to the variance are $v_i = x_i^2$. The standard deviation S of the variance values is given by

$$S^2 = \langle (v_i - \bar{v})^2 \rangle = \langle v^2 \rangle - \bar{v}^2 \tag{A-1}$$

and the error ε_v in the mean variance estimate can be taken as

$$\varepsilon_v^2 = (\langle v^2 \rangle - \bar{v}^2)/(N - 1) \tag{A-2}$$

where N is the number of independent values in the total of N values of x. Since $\bar{v} = \sigma^2$ and $\langle v^2 \rangle = \langle x^4 \rangle = \beta \sigma^4$, where β is the kurtosis of the x distribution (i.e. $\beta = \langle x^4 \rangle / \sigma^4$), then (A-2) becomes

$$\varepsilon_v^2 = \sigma^4 (\beta - 1)/(N - 1) \tag{A-3}$$

Now the error ε_σ in the mean σ value is related to ε_v by

$$(\sigma \pm \varepsilon_\sigma)^2 = \bar{v} \pm \varepsilon_v \tag{A-4}$$

but, from expansion of the left side of (A-4)

$$(\sigma \pm \varepsilon_\sigma)^2 \simeq \sigma^2 \pm 2\varepsilon_\sigma \sigma \tag{A-5}$$

where the second order term in ε_σ has been neglected. Since $\bar{v} = \sigma^2$, then it is

81

apparent from combination of (A-4), (A-5), and (A-3) that

$$\varepsilon_\sigma = \varepsilon_v/2\sigma = (\sigma/2)[(\beta - 1)/(N - 1)]^{1/2} \qquad (A-6)$$

The use of the divisor $N - 1$ in (A-2) means that the error is of the nature of an error of the mean. Thus ε_σ from (A-6) gives an error which would represent the range of deviation of the mean values obtained from comparable data sets each made up of N independent values.

REFERENCES

1. Justus, C. G. and A. Woodrum, Atmospheric Pressure, Density, Temperature, and Wind Variations Between 50 and 200 Km, NASA CR-2062, 1972.

2. Lindzen, R. S., and S. Chapman, Atmospheric Tides, Space Sci. Rev., 10 (1), 3 - 188, 1969.

3. Deland, R. J., and K. W. Johnson, Month. Wea. Rev., 96, 12, 1968.

4. Woodrum, A., and C. G. Justus, Measurement of the Irregular Winds in the Altitude Region near 100 Kilometers, J. Geophys. Res., 73 (23), 7535 - 7537, 1968.

5. Justus, C. G., Distribution and Structure of Irregular Winds near 100 Kilometers, J. Geophys. Res., 75 (12), 2171 - 2178, 1970.

6. Lumley, J. C., and H. A. Panofsky, The Structure of Atmospheric Turbulence, John Wiley & Sons, New York, 1964.

7. Lin, C. C., Statistical Theories of Turbulence, Princeton Univ. Press, New Jersey, 1961.

8. Avara, E. P., and B. T. Miers, The Noise Characteristics of Selected Wind and Temperature Data from 30 - 65 Km, ECOM-5402, 1971.

9. Moseley, W. B., Turbulent Velocity Distributions in the Upper Atmosphere, Georgia Tech Ph.D. Thesis, 1968.

10. Spizzichino, A., Private communicaton of Garchy meteor wind data, see also Spizzichino, A., and I. Revah, Space Research, 8, 679, 1967.

11. Barnes, A. A., Private Communication of Durham, N. H. Meteor Wind Data, see also Barnes, A. A., and J. J. Pazniokas, Results from the AFCRL Radar Meteor Trail Set, AFCRL-72-0185, 1972.

12. Pokrovskiy, G. B., et al., Izv. Atmos. and Ocean Phys., 5, 631, 1969.

13. Groves, G. V., J. Atmos. Terres. Phys., 16, 344, 1959.

14. Hines, C. O., Can. J. Phys., 38, 1441, 1960.

15. Kochanski, A., J. Geophys. Res., 69, 3651, 1964.

16. Dutton, J. A., and G. H. Fichtl, J. Atmos. Sci., 26, 241, 1969.

17. Miller, E. B., Atmospheric Density Variations Related to Internal Gravity Waves, NASA CR-61359, 1971.

18. Hoxit, Lee. R., and Robert M. Henry, Diurnal and Annual Temperature Variations in the 30-60Km Region as Indicated by Statistical Analysis of Rocketsonde Temperature Data, Proceedings of International Conference on Aerospace and Aeronautical Meteorology, Washington, D. C., 149-157, May 22-26, 1972.

19. Woodrum, Arthur, and C. G. Justus, Tidal Variations of Wind Components and Thermodynamic Variables in the 45 to 60 Km Height Range, paper presented to the fifty-third annual meeting of the American Geophysical Union in Washington, D. C., April 19, 1972.

20. Beyers, N. J., B. T. Miers, and R. J. Reed, Diurnal Tidal Motions Near the Stratopause during 48 Hours at White Sands Missile Range, J. Atmos. Sci., 23, 325, May 1966.

21. Miers, Bruce T., Wind Oscillations Between 30 and 60 Km Over White Sands Missile Range, New Mexico, J. Atmos. Sci., 22, 382, July 1965.

22. Reed, Richard J., Semidiurnal Tidal Motions between 30 and 60 Km, J. Atmos. Sci., 24, 315, May 1967.

23. Reed, Richard, J., Donald J. McKenzie, and Joan C. Vynerberg, Further Evidence of Enhanced Diurnal Tidal Motions near the Stratopause, J. Atmos. Sci., 23, 247, March 1966.

24. Reed, Richard J., Donald J. McKenzie, and Joan C. Vynerberg, Diurnal Tidal Motions between 30 and 60 Kilometers in Summer, J. Atmos. Sci., 23, 416, July 1966.

25. Reed, Richard J., Michael J. Oard, and Marya Sieminski, A Comparison of of Observed and Theoretical Diurnal Tidal Motions Between 30 and 60 Kilometers, Monthly Weather Rev., 97, 456, June 1969.

26. Harris, Miles F., Frederick G. Finger, and Sidney Teweles, Diurnal Variation of Wind, Pressure, and Temperature in the Troposphere and Stratosphere over the Azores, J. Atmos. Sci., 19, 136, March 1962.

27. Angell, J. K., and J. Korshover, The Biennial Wind and Temperature Oscillations of the Equatorial Stratosphere and Their Possible Extension to Higher Latitudes, Monthly Weather Review, 90 (4), April 1962.

28. Angell, J. K., and J. Korshover, Harmonic Analysis of the Biennial Zonal-Wind Temperature Regimes, Monthly Weather Review, 91, Oct. - Dec. 1963.

29. Angell, J. K., and J. Korshover, Quasi-Biennial Variations in Temperature Total O Zone, and Tropopause Height, J. Atmos. Sci., 21, Sept. 1964.

30. Reed, Richard J., The Quasi-Biennial Oscillation of the Atmosphere Between 30 and 50 Km Over Ascension Island, J. Atmos. Sci., 22, May 1965.

31. Angell, J. K., and J. Korshover, A Note on the Variation with Height of the Quasi-Biennial Oscillation, J. Geophys. Res., 70 (6), Aug. 15, 1965.

32. Shah, G. M., and W. L. Gadson, The 26-Month Oscillation in Zonal Wind and Temperature, J. Atmos. Sci., 23, Nov. 1966.

33. Rahmatullah, M., Quasi-Biennial Oscillation and Atmospheric Structure in the Stratosphere and Mesosphere, Space Research VII, 1968.

34. Cole, A. E., Periodic Oscillations in the Tropical and Subtropical Atmosphere at Levels Between 25 and 80 Km, Space Research VII, 1968.

35. Gregory, J. B., Dynamical Coupling from Below, Report to IUCSTP, Working Group 10, Feb. 1971.

36. Reed, R. J., Zonal Wind Behavior in the Equatorial Stratosphere and Lower Mesosphere, J. Geophys. Res., 71 (18), Sept. 1966.

37. Charney, J. G., and P. G. Drazin, Propagation of Planetary – Scale Disturbances from the Lower into the Upper Atmosphere, J. Geophys. Res., 66 (1) Jan. 1961.

38. Lindzen, R. S., Planetary Waves on Beta – Planes, Monthly Weather Rev., 95, 441, July 1967.

39. Dickinson, Robert E., Vertical Propagation of Planetary Rossby Waves through an Atmosphere with Newtonian Cooling, J. Geophys. Res., 74 (4), Feb. 15, 1969.

40. Matsuno, Tarah, Vertical Propagation of Stationary Planetary Waves in the Winter Northern Hemisphere, J. Atmos. Sci., 27, Sept. 1970.

41. Yanai, M., and T. Maruyama, J. Meteor. Soc., Japan, 44, 291, 1966.

42. Wallace, J. M., and V. E. Kousky, J. Atmos. Sci., 25, 900, 1968.

43. Holton, J. R., and R. S. Lindzen, An Updated Theory of the Quasi-Biennial Cycle of the Stratosphere, J. Atmos. Sci., 29, 1076-1080, 1972.

44. Hicks, J. E., and C. G. Justus, J. Geophys. Res., 75, 5565, 1970.

45. Minzner, R. A., and D. Morgenstern, GCA Tech. Rept., 68-1-N, 1968.

46. Testud, J. and G. Vasseur, Gravity Waves Generated During Magnetic Substorms, presented at the International Symposium on Waves in the Upper Atmosphere, Toronto, Jan. 1970.

47. Smith, L. B., J. Geophys. Res., 73, 4959, 1968.

48. Sprenger, K., and R. Schminder, J. Atmos. Terr. Phys., 31, 217, 1969.

49. Woodbridge, D. D., Planet. Space Sci., 19, 821, 1971.

50. Noonkester, V. R., J. Geophys. Res., 72, 1275, 1967.

51. Roberts, W. O., and R. H. Olson, Study of Lower Stratospheric Circulation Over North American following Geomagnetic Disturbances, IUGG Symposium, Moscow, Aug. 5, 1971.

52. Shapiro, R., J. Atmos. Sci., 29, 1213, 1972.

53. Smith, O. E., J. R. Redus, J. A. Forney, and M. J. Dash, Effects of Atmospheric Models on Space Shuttle Trajectories and Aerodynamic Heating, International Conf. on Aerospace and Aeronautical Meteorology, Washington, D. C., May 1972.

54. Daniels, G. E. (ed), Terrestrial Environment (Climatic) Criteria Guidelines for Use in Space Vehicle Development, 1971 Revision, NASA-TM-X-64589, May 1971.

55. Campbell, J. W., The Effect of Random Fluctuations in Atmospheric Density on Significant Space Shuttle Re-entry Parameters, International Conf. on Aerospace and Aeronautical Meteorology, Washington, D. C., May 1972.

56. Hicks, J. E., and C. G. Justus, A Numerical Simulation of Nearly Incompressible Stably Stratified Atmospheric Turbulent Diffusion, Sci. Rept. 1, NSF Grant GA-29213, Sept. 1971.